Resolution Requirements for the Simulation of Deep Moist Convection

GEORGE H. BRYAN, JOHN C. WYNGAARD, AND J. MICHAEL FRITSCH

Department of Meteorology, The Pennsylvania State University, University Park, Pennsylvania

(Manuscript received 26 December 2002, in final form 2 April 2003)

ABSTRACT

The spatial resolution appropriate for the simulation of deep moist convection is addressed from a turbulence perspective. To provide a clear theoretical framework for the problem, techniques for simulating turbulent flows are reviewed, and the source of the subgrid terms in the Navier–Stokes equation is clarified.

For decades, cloud-resolving models have used large-eddy simulation (LES) techniques to parameterize the subgrid terms. A literature review suggests that the appropriateness of using traditional LES closures for this purpose has never been established. Furthermore, examination of the assumptions inherent in these closures suggests that grid spacing on the order of 100 m may be required for the performance of cloud models to be consistent with their design.

Based on these arguments, numerical simulations of squall lines were conducted with grid spacings between 1 km and 125 m. The results reveal that simulations with 1-km grid spacing do not produce equivalent squall-line structure and evolution as compared to the higher-resolution simulations. Details of the simulated squall lines that change as resolution is increased include precipitation amount, system phase speed, cloud depth, static stability values, the size of thunderstorm cells, and the organizational mode of convective overturning (e.g., upright towers versus sloped plumes). It is argued that the ability of the higher-resolution runs to become turbulent leads directly to the differences in evolution.

There appear to be no systematic trends in specific fields as resolution is increased. For example, mean vertical velocity and rainwater values increase in magnitude with increasing resolution in some environments, but decrease with increasing resolution in other environments. The statistical properties of the simulated squall lines are still not converged between the 250- and 125-m runs. Several possible explanations for the lack of convergence are offered. Nevertheless, it is clear that simulations with O(1 km) grid spacing should not be used as benchmark or control solutions for resolution sensitivity studies.

The simulations also support the contention that a minimum grid spacing of O(100 m) is required for traditional LES closures to perform appropriately for their design. Specifically, only simulations with 250- and 125-m grid spacing resolve an inertial subrange. In contrast, the 1-km simulations do not even reproduce the correct magnitude or scale of the spectral kinetic energy maximum. Furthermore, the 1-km simulations contain an unacceptably large amount of subgrid turbulence kinetic energy, and do not adequately resolve turbulent fluxes of total water.

A guide to resolution requirements for the operational and research communities is proposed. The proposal is based primarily on the intended use of the model output. Even though simulations with O(1 km) grid spacing display behavior that is unacceptable for the model design, it is argued that these simulations can still provide valuable information to operational forecasters. For the research community, O(100 m) grid spacing is recommended for most applications, because a modeling system that is well founded should be desired for most purposes.

1. Introduction

Continuing advances in computer resources now allow researchers to simulate convective systems with very high resolution. For example, it is possible to run a three-dimensional explicit simulation of a thunderstorm with 1-km grid spacing on a desktop computer overnight. Presently, horizontal grid spacing of order 1 km is generally considered sufficient to simulate deep moist convection. This rule of thumb has its basis in a long history of simulations in which O(1 km) grid spacing has been utilized [see, e.g., Wilhelmson and Wicker (2001) for a review]. This resolution also follows from an analysis of the scales associated with deep moist convection. A typical thunderstorm cell is of order 10 km in scale in all three directions. Thus, it has been argued that 1-km grid spacing is sufficient to resolve the basic thunderstorm structure.

On the other hand, a growing number of studies are finding a strong (and disturbing) sensitivity of results when using grid spacing smaller than 1 km. For example, Adlerman and Droegemeier (2002) found that simulations of supercell thunderstorms are very sensitive to horizontal resolution. Among other differences, they found that the number and duration of mesocyclone cycles changed as grid spacing was decreased

Corresponding author address: George H. Bryan, National Center for Atmospheric Research, Advanced Study Program, P. O. Box 3000, Boulder, CO 80307.
E-mail: gbryan@ucar.edu

from 2 km to 105 m. Other recent studies that have documented changes in results with grid spacing less than 1 km include Grabowski et al. (1998), Petch and Gray (2001), and Petch et al. (2002).

Since current massively parallel computing systems—particularly those at national supercomputing centers—now make it possible to simulate deep moist convection with grid spacing on the order of 100 m, it is natural to ask whether such high resolution is necessary, and at what point simulations of convective processes can be considered ''well resolved.'' Although 1-km grid spacing captures the basic cumulonimbus structure, it is clearly insufficient to resolve any intracloud motions, such as the commonly observed sub-cloud-scale eddies that comprise much of the makeup of convective clouds. It is not clear whether resolving these structures affects the fidelity of the overall storm simulation. It is often assumed that traditional subgrid turbulence parameterizations are accounting for these motions, although it has never been established that these techniques are truly appropriate for this purpose. In this context, a clear theoretical framework to guide the modeling community in configuring cloud models in a manner that will include turbulent processes is desirable.

This paper provides some guidance in the debate over adequate resolution via an examination of subgrid turbulence modeling. To this end, sections 2 and 3 provide a theoretical background for three-dimensional numerical modeling of turbulent flows. In support of the theory, numerical simulations have been conducted with grid spacings from 1 km to 125 m. An analysis of the results in sections 4 and 5 reveals potential problems with the commonly used 1-km grid spacing. A summary of results is provided in section 6 and a recommendation for what constitutes adequate resolution is presented in section 7. Suggestions for future research are discussed in section 8.

2. Simulating turbulent flows

a. Direct numerical simulation

The fundamental challenges of simulating turbulent flows can be illustrated via the Navier–Stokes momentum equation for incompressible flow,

$$\frac{\partial u_i}{\partial t} = -\frac{\partial u_i u_j}{\partial x_j} - \frac{1}{\rho}\frac{\partial p}{\partial x_i} + \nu\frac{\partial^2 u_i}{\partial x_j \partial x_j}, \tag{1}$$

where u_i is velocity,[1] p is pressure, ρ is density, and ν is molecular kinematic viscosity (which is assumed to be constant). The terms involving buoyancy and the Coriolis force have been neglected, since they do not affect the conclusions drawn here. Equation (1) is valid for all scales of motion, from planetary-scale waves of order 10^7 m to dissipative eddies of order 10^{-4} m (or less). If one wishes to simulate a turbulent flow using (1), it is necessary to resolve *all* scales of motion, including the smallest dissipative eddies; this is because energy is generated primarily by the largest eddies in the flow, and is dissipated at the smallest scales. It is not possible to faithfully simulate turbulent processes without accounting for these two effects (Lilly 1967).

The scale of the dissipative eddies—the Kolmogorov microscale, η—depends only on ν and the rate of dissipation per unit mass (ε),

$$\eta = \left(\frac{\nu^3}{\varepsilon}\right)^{1/4} \tag{2}$$

(Kolmogorov 1941). Since $\varepsilon \cong u^3/l$, where l and u are the length and velocity scales of the energy-containing eddies (Tennekes and Lumley 1972), it follows that

$$\frac{l}{\eta} \sim R_t^{3/4}, \tag{3}$$

where $R_t = ul/\nu$ is the turbulence Reynolds number. For deep moist convection, u is of order 10 m s^{-1} and l is of order 10^4 m. Thus, R_t is of order 10^{10}. Based on (3), the scale of the dissipative eddies (η) is about 3×10^{-4} m, meaning that approximately 0.1-mm grid spacing would be required to resolve all motions in deep moist convection. This is clearly beyond the capabilities of computers available today, or in the foreseeable future. Corrsin (1961) is usually acknowledged as the first to point out the hopelessness of directly simulating large Reynolds number flows. An alternative to direct numerical simulation of deep moist convection is necessary.

b. Filtered Navier–Stokes equation

As first proposed by Lilly (1967), in lieu of reproducing all scales of a turbulent flow, one can integrate a flow in which small-scale details are removed from the solution. If the scale of the filtering operator is much larger than η, it is possible to have manageable grids that can be integrated with available computers. Deardorff (1970a) was the first to use this approach. He applied it to turbulent channel flow, removing the small scales by formally averaging the solution fields over the elemental volume of the numerical grid mesh. Leonard (1974) generalized this to spatial filtering and discussed several types of filter functions, including the ''top-hat'' form corresponding to Deardorff's grid-volume averaging.

A governing equation for a filtered flow can be derived by spatially filtering (1). The type of filter used is not important here, as long as the filtering operation commutes with differentiation. The result is

$$\frac{\partial u_i^r}{\partial t} = \frac{\partial (u_i u_j)^r}{\partial x_j} - \frac{1}{\rho}\frac{\partial p^r}{\partial x_i} + \nu\frac{\partial^2 u_i^r}{\partial x_j \partial x_j}, \tag{4}$$

where a superscript r refers to a resolved-scale (technically, filtered) variable. The viscous term [last on the

[1] Einstein summation notation is used.

right-hand side of (4)] can be neglected, since the scales at which it is important have been removed.

Equation (4) cannot be integrated directly since it involves an unknown term, $(u_i u_j)^r$. However, this term can be rearranged by noting that u_i is the sum of resolved-scale and subgrid-scale components,[2]

$$u_i = u_i^r + u_i^s, \tag{5}$$

so the unknown term can be written as

$$(u_i u_j)^r = (u_i^r u_j^r)^r + (u_i^r u_j^s)^r + (u_i^s u_j^r)^r + (u_i^s u_j^s)^r. \tag{6}$$

The first term on the right-hand side of (6) can be determined on the model grid. However, it is often inconvenient to do so, especially when the numerical model is based on finite differencing techniques. This is because filtering is rarely carried out explicitly in spatially gridded finite-difference-based models [see, e.g., the discussion in the introduction of Mason and Brown (1999)]. More specifically, the first term on the right-hand side of (6) requires multiplying two filtered fields, and then filtering the resulting product. This can be accomplished relatively easily in a spectral or psuedo-spectral model, [as is done in the model of Moeng (1984)], but cannot be carried out in a numerical model in which the filtering is implied. Therefore, (6) is often rewritten as

$$\begin{aligned}(u_i u_j)^r &= u_i^r u_j^r - u_i^r u_j^r + (u_i^r u_j^r)^r + (u_i^r u_j^s)^r + (u_i^s u_j^r)^r \\ &\quad + (u_i^s u_j^s)^r \\ &= u_i^r u_j^r + \tau_{ij}\end{aligned} \tag{7}$$

where

$$\begin{aligned}\tau_{ij} &= [(u_i^r u_j^r)^r - u_i^r u_j^r] + [(u_i^r u_j^s)^r + (u_i^s u_j^r)^r] \\ &\quad + (u_i^s u_j^s)^r.\end{aligned} \tag{8}$$

The first bracketed term on the right-hand side of (8) is the Leonard stress, the second bracketed term is the cross-term stress, and the final term is the Reynolds stress.

The final form of the filtered Navier–Stokes equation can thus be written as

$$\frac{\partial u_i^r}{\partial t} = -\frac{\partial u_i^r u_j^r}{\partial x_j} - \frac{\partial \tau_{ij}}{\partial x_j} - \frac{1}{\rho}\frac{\partial p^r}{\partial x_i}. \tag{9}$$

All variables in (9) are available on the model grid except for τ_{ij}, which must be accounted for via parameterization. The purpose of this analysis is not to explain how τ_{ij} is approximated and (9) is integrated; indeed, there are many methods for doing so [see, e.g., section 5.4 in Tannehill et al. (1997)]. Rather, the main point to be stressed here is that the Navier–Stokes equation, (1), cannot be integrated on a computer due to computer resource limitations. A new equation, the filtered Navier–Stokes equation, is developed that *can* be integrated with available resources. The new equation, (9), contains an unknown term, τ_{ij}, that must be parameterized. This is the essence of the ''turbulence closure problem'' for cloud-resolving models.

The use of (9) with a parameterization for τ_{ij} is now known as large-eddy simulation (LES). LES has been used successfully to simulate many types of turbulent flows, including geophysical and engineering flows. Although it is not widely acknowledged, cloud-resolving models have used LES techniques for decades. For this reason, LES will be addressed in the remainder of this study.

3. Large-eddy simulation

The traditional[3] subgrid model for LES plays two roles. The first is to specify the subgrid flux. In (9), τ_{ij} can be interpreted as the subgrid kinematic momentum flux with $u_i^r u_j^r$ being the resolved kinematic momentum flux. The second role is to transfer kinetic energy from resolved scales to unresolved scales. In the inertial subrange, the second role is considerably more important, because the small eddies carry negligible flux but are key players in the cascade of energy to smaller scales. For this reason, traditional LES of large R_t flows assumes that the grid spacing (Δ) is much larger than the small dissipative eddies of scale η, but much smaller than the large energy-containing eddies of scale l, that is,

$$l \gg \Delta \gg \eta. \tag{10}$$

A grid spacing within these two scales ensures that the simulation resolves the eddies that contain most of the kinetic energy and carry most of the flux in turbulent flows: hence, the name large-eddy simulation.

For a more thorough review of LES, the reader is referred to Rogallo and Moin (1984) and Moeng (1984). For the purposes of this work, it is sufficient to present two aspects of (10) that are relevant to the issue of adequate resolution:

Assumption 1—The grid spacing (Δ) is well within the inertial subrange; and

Assumption 2—the scale of the phenomenon to be simulated (l) is *much* larger than the grid spacing[4] (Δ).

[2] Technically, these two components should be referred to as filtered instead of resolved scale, and as subfilter scale instead of subgrid scale. However, we will make use of the common terminology here.

[3] In this study, the terms traditional subgrid model, traditional LES, and traditional closure refer specifically to LES modeling with the Smagorinsky–Lilly inertial-subrange-based closure (Smagorinsky 1963; Lilly 1967). This includes the turbulence kinetic energy scheme of Deardorff (1980).

[4] Actually, Δ here should be the model's filter scale, not the model's grid spacing. As noted by Mason and Brown (1999), the filter scale is slightly larger than the grid spacing, but of the same order of magnitude. For this qualitative discussion, we will assume that the filter scale and the grid scale are approximately equal.

In the inertial subrange there is a scale-independent mean rate of transfer of kinetic energy per unit mass, from large scales to smaller ones, destined to be dissipated at rate ε in the smallest eddies of scale η. In LES, it is considered sufficient to resolve the large energy-containing eddies while parameterizing the rate of energy transfer to subgrid scales. In other words, it is assumed that one end of the energy cascade is resolved on the model grid, and the other end can be accounted for through a subgrid model.

The second assumption can be interpreted following Wyngaard (1982). Specifically, if the effect of the subgrid eddies on the resolved ones is represented through an eddy diffusivity K, then one expects $K \sim u^s l^s$, the product of the velocity and length scales of the subgrid turbulence. If the filter scale Δ lies in the inertial subrange, $l^s \sim \Delta$ and $u^s \sim (\varepsilon\Delta)^{1/3}$ (Tennekes and Lumley 1972). Thus, $K \sim \varepsilon^{1/3}\Delta^{4/3}$ and the resolved flow has a Reynolds number of order

$$R_t \sim \frac{ul}{K} \sim \frac{ul}{\varepsilon^{1/3}\Delta^{4/3}}. \tag{11}$$

Since $\varepsilon \sim u^3/l$, this becomes

$$R_t \sim \left(\frac{l}{\Delta}\right)^{4/3}. \tag{12}$$

For the resolved flow to be turbulent it is necessary that $R_t \gg 1$, which requires $l \gg \Delta$.

It has been unclear whether cloud-resolving models (CRMs) with $\Delta \sim 1$ km satisfy assumptions 1 and 2. Nevertheless, the subgrid turbulence closures used in most CRMs have been taken directly from LES models. The main reference used to justify this design appears to be Klemp and Wilhelmson (1978). Several arguments were put forth by Klemp and Wilhelmson in support of this strategy, although they acknowledged that it may not be entirely appropriate to do so. For example, they note that their subgrid closure is ''. . . based on the existence of a grid scale within the inertial subrange and with present resolution [1 km] this requirement is not satisfied.'' The computational resources available at the time made it impossible for Klemp and Wilhelmson to utilize higher resolution. Furthermore, it is *still* unclear where the inertial subrange begins in deep moist convection. The most relevant studies are probably those of Droegemeier et al. (1994, 1996) and Lilly et al. (1998); they did not find clear evidence of an inertial subrange in simulations of supercell thunderstorms, even with grid spacing as small as 250 m.

An evaluation of the two relevant length scales (l and Δ) used in planetary boundary layer (PBL) modeling may provide valuable guidance for the present study. LES has been used successfully to study the PBL for more than 30 yr, beginning with the studies of Deardorff (1970b,c). In these studies, $l \sim 1000$ m (the depth of the boundary layer), and $\Delta \sim 10$ m (a typical order-of-magnitude grid spacing). Since $l/\Delta \sim 100$, assumption 2 is satisfied, R_t is large, and the simulated flow is turbulent. Note that even though Reynolds numbers for LES studies are much smaller than geophysical values of R_t (i.e., 10^2–10^3 as opposed to 10^8–10^{10}), one still expects the simulated flow to be representative of the physical counterpart due to Reynolds number similarity (see, e.g., Tennekes and Lumley 1972). That is, once a critical Reynolds number is exceeded, the inertial forces in the flow are much larger than the viscous forces, and the mean properties of the flow cease to change significantly with further increases in R_t.

In contrast to the PBL studies, for many cloud modeling studies $l \sim 10$ km (a typical depth and width of a thunderstorm) and $\Delta \sim 1$ km. Since l/Δ is only ~ 10, assumption 2 is probably not satisfied. Thus, the Reynolds number could be too small for the flow to be fully turbulent.

Considering that a l/Δ ratio of about 100 evidently works well for LES studies of the PBL, it seems reasonable to use this relationship as guidance for the cloud modeling community. For $l \sim 10$ km, *the relationship suggests that 100-m grid spacing may be necessary for it to lie in the inertial subrange and for the LES closure to be appropriate for simulations of deep moist convection.* One primary goal of the following simulations was to simulate deep moist convection with grid spacing of order 100 m to test this hypothesis.

Before proceeding, it is noted that Droegemeier et al. (1997) came to a similar conclusion based on their supercell simulations. Using 2-km grid spacing, the simulated storm was rather smooth and ''unremarkable'' in terms of details that are expected in turbulent overturning. In contrast, a simulation with 250-m grid spacing contained much finer detail. Droegemeier et al. (1997) conclude that with 250-m grid spacing the turbulent features in deep moist convection are beginning to be explicitly resolved. The studies of Droegemeier et al. (1994, 1996, 1997) and Lilly et al. (1998) also conclude that more work in the area is warranted. For example, several statistics computed from their simulations (such as energy spectra) did not show convergence between resolutions, suggesting the need to explore simulations with grid spacing smaller than 250 m. The lack of a clear inertial subrange in their analyses is also unsettling, and further supports the need to explore higher resolution.

The recent study of Stevens et al. (2002) also supports the arguments put forth in this section. For numerical simulations of shallow cumulus convection, they found that decreasing the horizontal grid spacing to 20 m or less was required to adequately resolve entrainment processes. By comparing output from simulations with horizontal resolutions between 80 and 10 m, they argue that resolution of $O(10\text{ m})$ is ''required to obtain meaningful cloud statistics'' of shallow cumulus. Given a boundary layer depth (l) of ~1500 m, their simulations support our argument in favor of a l/Δ ratio of about 100.

4. Design of numerical simulations

In this study, numerical simulations of squall lines are utilized to investigate the turbulent properties of deep moist convection. The quasi-two-dimensional structure of squall lines is advantageous for this purpose, since the numerous deep convective cells in the along-line direction provide many realizations of turbulent overturning at any instant in time. The implied statistical homogeneity in the along-line direction facilitates the statistical analyses to be presented later, which are used to assess the appropriateness of LES modeling.

The choice to simulate squall lines also allows for comparison with the study of Weisman et al. (1997). Their study has since served as the primary justification for the use of *O*(1 km) grid spacing to simulate deep convective processes. Due mainly to limitations in computing resources, the highest-resolution simulation of Weisman et al. (1997) utilized 1-km grid spacing, which they used as the ''ground truth'' to evaluate coarser-resolution simulations. One goal of this new study is to explore the resolution dependence of squall-line simulations at an order of magnitude higher resolution, that is, with grid spacing of *O*(100 m). Furthermore, the validity of using *O*(1 km) simulations as truth is also addressed with these new simulations.

The numerical model used for this study is described in Bryan and Fritsch (2002) and Bryan (2002). The governing equations are integrated using the Runge–Kutta technique as formulated for compressible models by Wicker and Skamarock (2002). All simulations use fifth-order spatial discretization for the advection terms. No additional artificial diffusion is applied. The subgrid turbulence parameterization is nearly identical to that presented in Deardorff (1980). Simulations were conducted using horizontal grid spacing of 1 km, and 500, 250, and 125 m. For the 1-km simulation, the vertical grid spacing was 500 m. For all other resolutions, the vertical grid spacing was the same as the horizontal.

The model domain is 300 km long in the across-line (west to east) direction, and is 60 km long in the along-line (south to north) direction. The lateral boundary conditions in the across-line direction are open-radiative, and permit gravity waves to exit the domain with minimal reflection. The lateral boundary conditions in the along-line direction are periodic, which allows the squall line to extend across the entire domain in this direction. The vertical extent of the domain is 18 km. The lower boundary is a flat, rigid surface, as is the upper boundary. A Rayleigh damping layer (Durran and Klemp 1983) is applied in the upper 4 km of the domain to damp gravity waves that propagate upward above the convection.

The squall line is initiated with a north–south line thermal. The perturbation has a maximum amplitude of 2 K, and is located 1.5 km above ground. The perturbation decreases to zero in a radius of 10 km horizontally and 1.5 km vertically. Small potential temperature perturbations of maximum amplitude 0.2 K are inserted into the line thermal to allow three-dimensional flows to develop. Over the remainder of the domain the initial conditions are horizontally homogeneous.

The design of the simulations is similar to that of Weisman et al. (1997), except that a line thermal is used to initiate convection rather than a surface-based cold pool. To build upon their work, the same analytic temperature and moisture profiles (Weisman and Klemp 1982) were used in all simulations. Furthermore, the three wind profiles used by Weisman et al. (1997) are also used here. One features 17.5 m s^{-1} of across-line shear over the lowest 2.5 km, and will hereafter be referred to as the strong-shear profile; the second has 10 m s^{-1} of shear over the lowest 2.5 km, and will be referred to as the weak-shear profile; the third has 25 m s^{-1} of shear over the lowest 5.0 km, and will be referred to as the deep-shear profile. There is no initial flow in the along-line direction. Experience has shown that these three wind profiles allow the development of a broad range of convective organization. This is important for the present study, since it allows us to address whether the results are dependent on a specific mode of convective overturning.

The simulations use the Kessler (1969) microphysical model (as presented in Klemp and Wilhelmson 1978), which considers only the liquid phase. Simulations with ice processes would have approximately doubled the computational requirements; although this was within the capability of the computing facilities available for this study, it was decided that the limited resources would be better spent on a larger number of runs with different environmental conditions and resolutions. No atmospheric radiative heating is considered, nor are there any surface fluxes. This design allows the environmental conditions to remain steady during the simulation. Free-slip conditions are specified at the lower and upper boundaries. The Coriolis force is not considered, due to the (relatively) short simulation time of 180 min.

The grid mesh for the 125-m simulations is $2400 \times 480 \times 144$ grid points, or 1.66×10^8 total grid points. This is (obviously) a large problem. Fortunately, today's massively parallel computing systems make this problem tractable. The simulations were integrated using 128 processors of the National Center for Atmospheric Research IBM SP RS/6000. The total wall-clock time for the integration was 84 h, which is a reasonable amount of time to wait for a simulation. Considering the ongoing advancements in computing power, we suggest that simulations using *O*(100 m) grid spacing are not as unreachable as most probably assume.

5. Results

a. Instantaneous fields

Overall, it has been found that details of the simulated squall lines can change significantly as resolution is in-

TABLE 1. Sensitivity of various properties to resolution and shear. All values were calculated 180 min into the simulations.

Grid spacing (m)	Rainfall ($\times 10^9$ kg)	Maximum cloud top (km)	Maximum lapse rate (K km^{-1})	Avg x-location of surface gust front (km)
$U_s = 10$ m s^{-1} over 2.5 km (weak shear)				
1000	94.1	14.75	15.1	219.6
500	98.5	14.75	24.3	220.7
250	96.5	14.38	31.8	222.6
125	95.3	14.06	58.8	216.0
$U_s = 17.5$ m s^{-1} over 2.5 km (strong shear)				
1000	96.8	15.75	14.8	203.3
500	97.9	15.25	18.8	207.7
250	98.5	14.38	32.7	213.7
125	94.7	14.06	52.4	213.2
$U_s = 25$ m s^{-1} over 5 km (deep shear)				
1000	90.9	14.25	18.2	191.4
500	110.8	15.25	17.3	198.4
250	105.5	15.63	31.6	198.2
125	107.1	14.31	63.8	199.7

creased, including precipitation distribution and amount, convective cell structure, and mesoscale flow patterns. Depending on the intended use of a numerical simulation, the changes may be more significant for some purposes than others. For example, values of total precipitation, cloud depth, and gust front speed (used as a proxy for system propagation speed) vary by 5%–20% for all three shear profiles studied here (Table 1). On the other hand, the maximum lapse rate (i.e., the maximum value of $\Gamma = -\partial T/\partial z$ at any grid point in the domain) more than triples from the 1-km simulation to the 125-m simulation. Bryan (2002) used numerical simulations to investigate the thermodynamic properties of the convective region of squall lines; the conclusions drawn from a simulation with 1-km grid spacing would have differed significantly from conclusions drawn from a simulation with 125-m grid spacing. Bryan (2002) also showed that the high values of lapse rate (i.e., exceeding 40 K km^{-1}) are physical, and result from the lifting of moist absolutely unstable layers by intense updrafts in a process analogous to vertical divergence frontogenesis (see, e.g., Bluestein 1986, his Eq. 9.11, term 12).

The processes that cause these differences in squall-line structure and evolution are being investigated, as it is impossible to explain all of these results in one study. Nevertheless, in a general sense, we believe that the ability of the higher-resolution runs to become turbulent is playing a primary role in creating these differences. For example, the lower-resolution simulations often exhibit plumes of high equivalent potential temperature (θ_e) that rise from the pre-squall-line boundary layer in a relatively laminar manner (Fig. 1a). The subgrid temperature and moisture fluxes act to diffuse away this high θ_e plume, although these traditional subgrid terms were not specifically designed for this purpose. In contrast, the instantaneous fields in the higher-resolution simulations are significantly more turbulent (Fig. 1b). Thus, entrainment in updrafts is resolved in the higher-resolution simulations. Areas of high θ_e tend to be smaller and less coherent, as resolved turbulent eddies stretch and distort the θ_e field.

The results also suggest that the rule of thumb relating typical cumulonimbus size (~10 km) to the grid spacing required to resolve it (~1 km) can be inadequate in some instances. Output from the strong-shear simulation with 1-km grid spacing features thunderstorm cells of order 4–6 km in scale—the minimum resolvable by the grid (Fig. 2a). In contrast the simulation with 125-m grid spacing features cells about 1–2 km in scale (Fig. 2b). In some conditions, cells *are* observed to be of order 10 km in scale, such as supercell thunderstorms. Furthermore, the simulations initialized with the other two wind profiles exhibit cells larger than those presented in Fig. 2b. Nevertheless, 1-km grid spacing is clearly not sufficient to resolve thunderstorm cells in some environments.

The highest-resolution simulations have considerably more detail than their low-resolution counterparts—a result that is not surprising. Some features ''collapse'' onto the grid scale even with 125-m grid spacing, such as the gust front and sub-cloud-scale turbulent eddies. Again, this is a result that is expected for three-dimensional simulations of turbulent flow.

It could be argued that the general nature of the overturning is the same for the two simulations shown in Figs. 1–2. That is, the convective region is characterized as a collection of cumulonimbus clouds. However, this conclusion does not hold for all of the environments studied here. For example, the simulations with weak shear reveal markedly different overturning as resolution is changed. The 1-km simulation can be characterized as a series of convective towers that form rearward of the surface gust front (Fig. 3a). This state is found along the entire length of the squall line. In contrast, the 125-m simulation is dominated by sloped plumelike structures, with continuous streams of high θ_e air that rise from the pre-squall-line boundary layer to the upper troposphere (Fig. 3b). This plumelike mode of overturning is completely absent from the simulation with 1-km horizontal grid spacing, revealing that the mode of convective overturning can be different as resolution is increased. Although the plumelike overturning in Fig. 3b appears similar to that of Fig. 1a, cross sections taken along the line (not shown) reveal the same differences in turbulent nature as shown in Fig. 2. That is, the cell in Fig. 3b contains sub-cloud-scale turbulent overturning on both sides of the plume in the along-line direction, while the cell in Fig. 1a does not.

The differences in convective organization are illustrated further by an analysis of θ_e in midlevels. The 1-km simulation does not exhibit any undilute cores at 5 km above ground (Fig. 4a). In fact, it is difficult to identify the convective cells in the 1-km simulation, as well as where the convective region ends and the stratiform region begins. The 125-m simulation, on the other

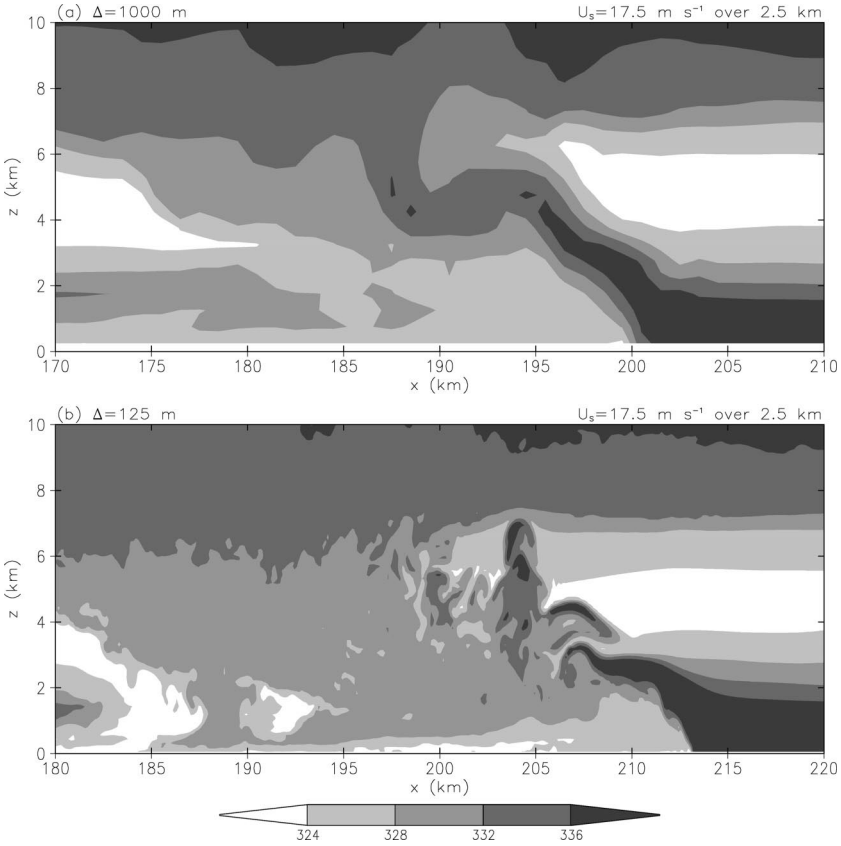

FIG. 1. Across-line cross sections of equivalent potential temperature (θ_e, in K) from strong-shear simulations at 180 min using (a) 1000-m grid spacing (at $y = 49$) and (b) 125-m grid spacing (at $y = 56$ km).

hand, exhibits clear cellular structures characterized by undilute cores. Of course, higher-resolution simulations should be expected to contain more details. A more appropriate comparison would use the high-resolution results downfiltered to the coarse-resolution grid. Such a procedure would better address the question of whether the two resolutions are producing equivalent structures. Toward this end, the θ_e field at 5 km from the 125-m simulation was filtered to the 1-km grid using a top-hat filter. Other filter types produced the same qualitative results. The filtered θ_e field still maintains a sense of undilute cores, and a single distinct convective region (Fig. 4c). Clearly, the 1-km simulation is not producing the same squall line as the 125-m simulation.

b. Mesoscale structure

Along-line-averaged values of vertical velocity (w) and rainwater mixing ratio (q_r) are shown in Figs. 5–7 for all shears and resolutions investigated here. These cross sections were calculated relative to the location of the surface gust front. For the strong-shear simulations, the mean vertical velocity pattern changes markedly as resolution is increased (Fig. 5). With 1-km grid spacing, high values of w extend continuously from the cold pool at low levels to the mid and upper levels. For example, the 3 m s^{-1} contour extends uninterrupted from near the surface to about 10 km. This pattern gives the appearance of a single stream of flow from the pre-squall-line boundary layer to the upper troposphere. As resolution is increased, the vertical velocity from the gust front becomes more clearly separated from the mid- and upper-level pattern. The region of w associated with the cold pool remains similar throughout the resolutions, though the w maximum is slightly larger in magnitude and slightly lower in height as resolution is increased. On the other hand, the mid- and upper-level w maximum weakens considerably, from ~4 m s^{-1} in the 1-km and 500-m simulations to only ~2 m s^{-1} in the 125-m simulation. This weaker w pattern arises even though maximum gridpoint values of w (i.e., instantaneous values) increase as resolution increases.

The mean q_r field in the strong-shear simulations also exhibits trends as resolution is increased (Fig. 5). Specifically, the q_r maximum weakens in magnitude and is located farther behind the gust front as resolution increases. The maximum height of the mean q_r field also lowers as resolution is increased, from ~12 km with 1-km grid spacing to ~10 km with 125-m grid spacing. This change in rainwater field is consistent with changes

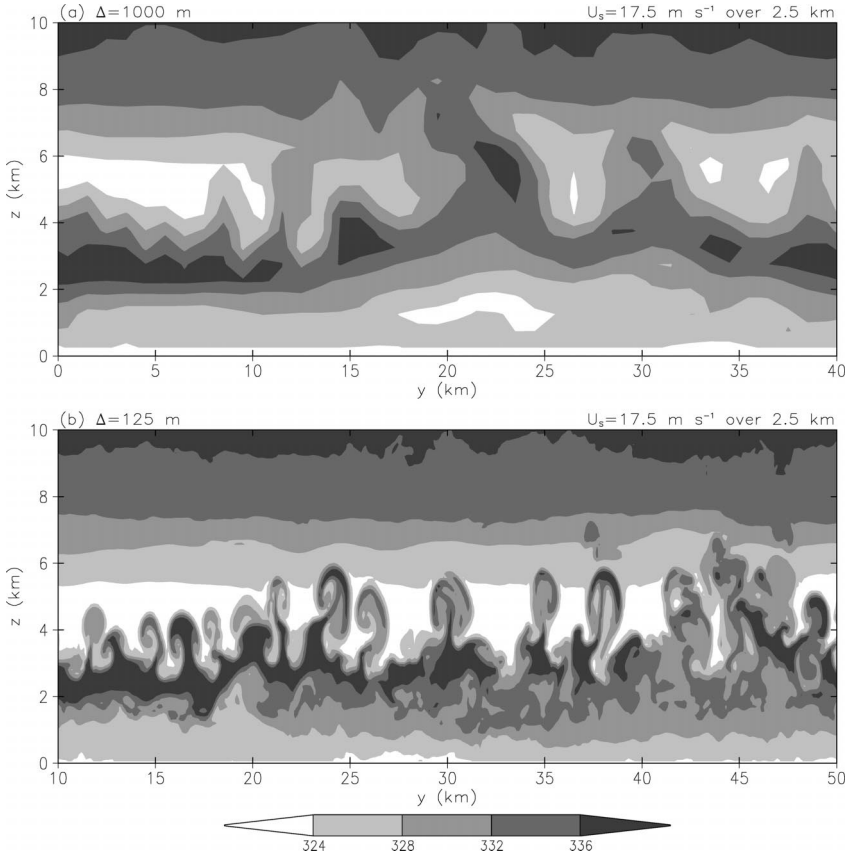

FIG. 2. The same as in Fig. 1 except along-line cross sections using (a) 1000-m grid spacing (at $x = 200$ km) and (b) 125-m grid spacing (at $x = 207$ km).

in the vertical velocity field, which also lowers as resolution is increased.

Mean fields from the simulation initialized with weak shear also change significantly as resolution is increased (Fig. 6). In this case, however, the trends are opposite to the trends from the strong-shear simulation. For example, the mean vertical velocity increases in value and in height as resolution increases. The rainwater field also generally increases in magnitude and extent (again, opposite the trend in the strong shear simulations). Based on these results, it does not seem likely that one could correct systematic biases in 1-km simulations in a simple manner.

Earlier, it was noted that the convective overturning in weak shear changed from a series of upright cells to a single undilute plume (as shown in Fig. 3) as resolution increased. The net effect of this change in convective mode is highlighted in the mean cross sections. Most notably, the 1-km simulation (Fig. 6a) fails to reproduce the overall pattern shown in the 125-m simulation (Fig. 6d). The 500- and 250-m runs do reproduce this structure. The instantaneous fields reveal that the 500- and 250-m simulations contain deep convective plumes that are similar to those in the 125-m simulation, though some details are different.

For the deep-shear simulations, the overall mesoscale structure of the squall line is similar over the various resolutions, although the magnitudes are markedly different (Fig. 7). In this case, both mean w and q_r increase in magnitude as resolution is increased. As in all other shear profiles, an exact (or even approximate) convergence has not been achieved as grid spacing changes from 250 to 125 m. This lack of convergence, also noted in the Droegemeier et al. (1994, 1996) studies, is unsettling. The statistical properties[5] of a turbulent flow are expected to converge at some resolution owing to (12) and Reynolds number similarity (Tennekes and Lumley 1972). That is, statistical properties of the flow (such as mean circulation, as expressed by line-averaged vertical velocity in Figs. 5–7) are not expected to change significantly after a critical Reynolds number is exceeded. The lack of convergence between 250- and 125-m simulations suggests the need for still further study at even higher resolution.

[5] As opposed to specific details of a turbulent flow, which have only been observed to converge under very controlled conditions such as a constant prescribed diffusion (e.g., as in Straka et al. 1993).

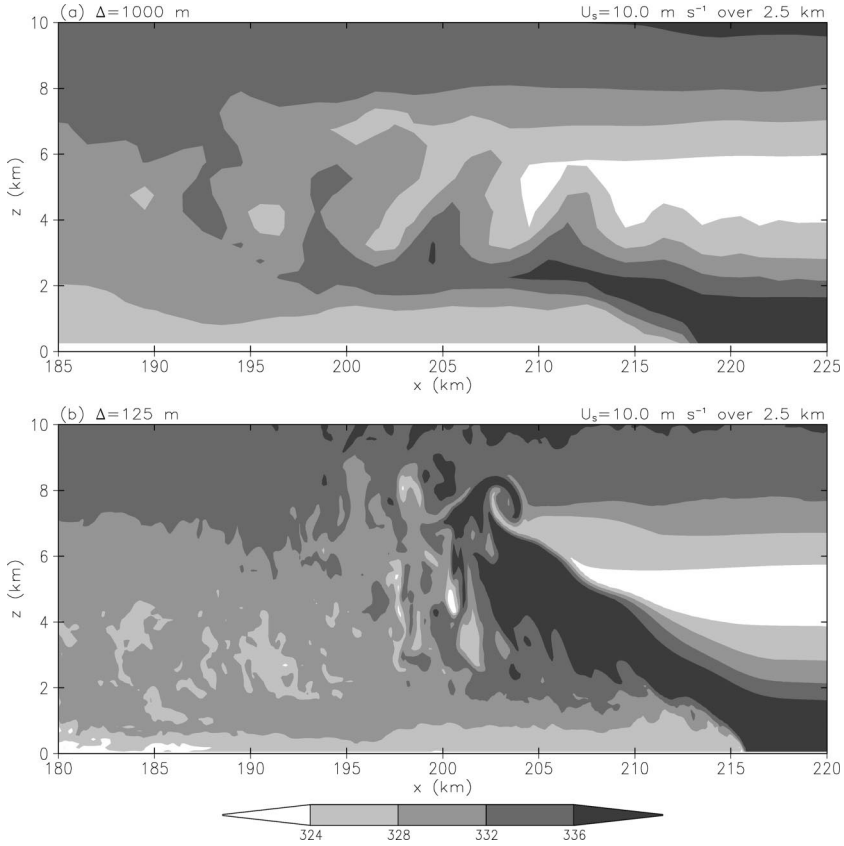

FIG. 3. Across-line cross sections of equivalent potential temperature (θ_e, in K) from weak shear simulations at 180 min using (a) 1000-m grid spacing (at $y = 45$) and (b) 125-m grid spacing (at $y = 49$ km).

c. Systemwide flux profiles

Weisman et al. (1997) calculated mean flux profiles over a large subdomain encompassing the entire convective system. Their simulations, using grid spacings from 12 km to 1 km, showed a convergence as grid spacing of order 1 km was approached. For most wind profiles, they found that simulations with 4-km horizontal grid spacing reproduced the structure and magnitude of mean flux profiles found with 1-km horizontal grid spacing, which was considered the benchmark (or control) solution.

To facilitate a comparison of the conclusions of Weisman et al. (1997) with those of the present study, the same flux profiles were calculated here. Profiles of vertical temperature flux $\langle w'\theta'\rangle$ and vertical kinematic momentum flux $\langle w'u'\rangle$ are presented in Figs. 8 and 9. Primes refer to deviations from the base state (i.e., the initial horizontally homogeneous conditions). The angular brackets signify horizontal averaging, which extends from 50 km ahead of the surface gust front to 100 km behind the surface gust front. This area is slightly smaller than that used by Weisman et al. (1997); theirs extended from 100 km ahead to 100 km behind of the gust front. A smaller averaging area was necessary here due to the smaller overall domain size. The missing 50 km here should not affect the patterns of heat and momentum flux, since the conditions this far ahead of the squall line are rather quiescent. However, the magnitude of the maximum values are expected to be larger in this study. The smaller extent of the domain in the along-line direction [60 km here, as opposed to 160 km in Weisman et al. (1997)] should not affect conclusions drawn here, although the flux profiles are less smooth due to the limited averaging area.

Results reveal that a convergence has clearly not been achieved at 1 km, since the flux profiles change with increases in resolution. The nature of the change is difficult to generalize, however. The exception is the strong-shear simulations, for which the vertical fluxes $\langle w'\theta'\rangle$ and $\langle w'u'\rangle$ decrease in magnitude as resolution increases (Figs. 8a and 9a). The change in $\langle w'u'\rangle$ is stunning, from a maximum of $\sim$6 m^2 s^{-2} with 1-km grid spacing to a maximum of $\sim$2.5 m^2 s^{-2} with 125-m grid spacing (Fig. 9a). For the other shear profiles, the fluxes tend to increase in magnitude as resolution is increased from 1 km to 500 m, and then decrease in magnitude from 500 to 250 m.

Results using 1-km grid spacing clearly have not con-

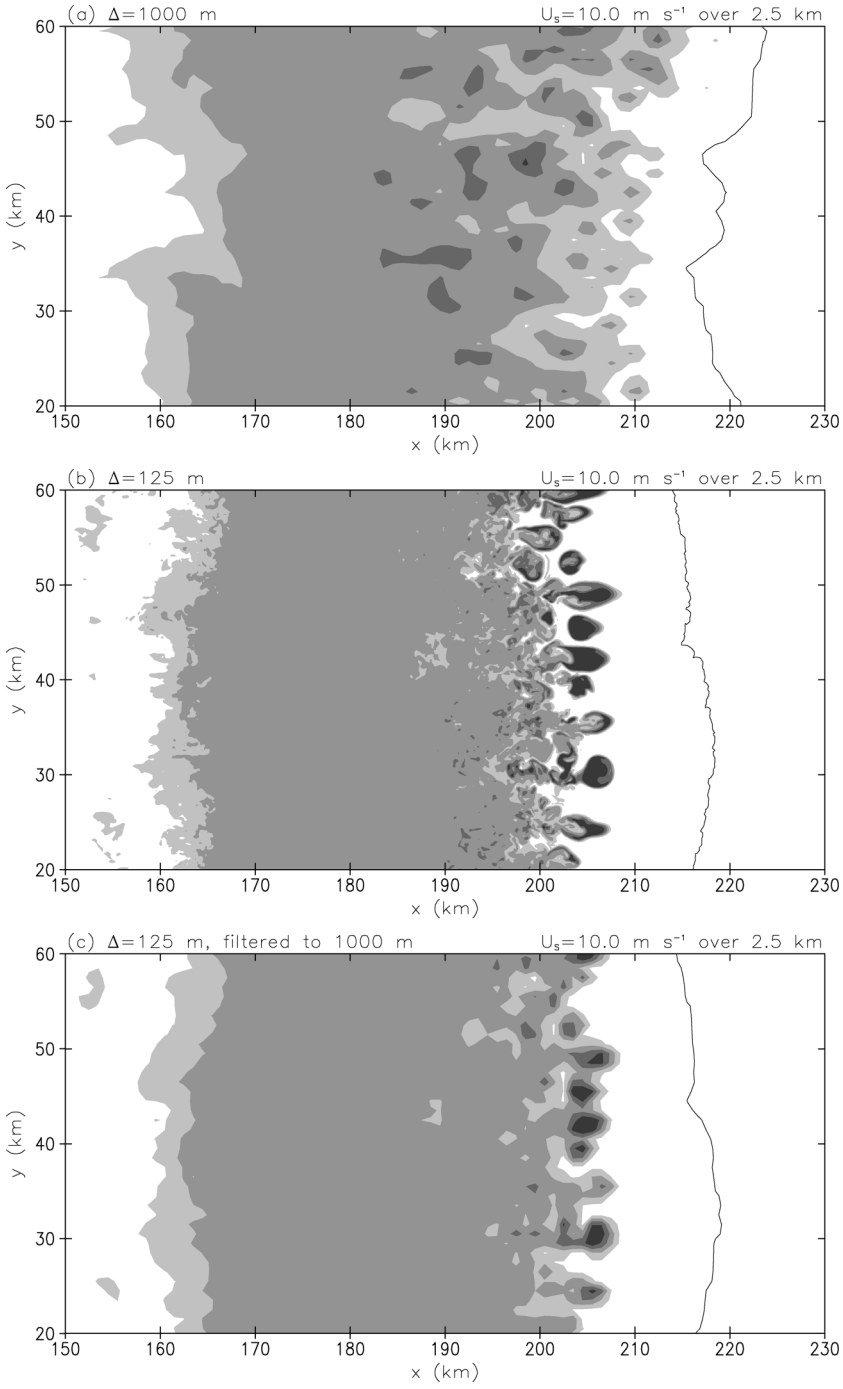

FIG. 4. Instantaneous views of θ_e (in K) at 5 km above ground from weak-shear simulations after 180 min using (a) 1000-m grid spacing, (b) 125-m grid spacing, and (c) 125-m grid spacing, where the results have been filtered to the 1000-m grid using a ''top hat'' filter. Shading is the same as in Figs. 1–3. The −1 K surface potential temperature perturbation is included as a black contour, which indicates the approximate position of the surface gust front.

verged. It is concluded that 1-km grid spacing cannot be used as truth in resolution sensitivity studies. However, the results presented here do not conclusively show that 125 m represents a converged solution, either.

d. Energy spectra

To determine whether the arguments made in section 3 are valid—that is, that grid spacing of order 100 m

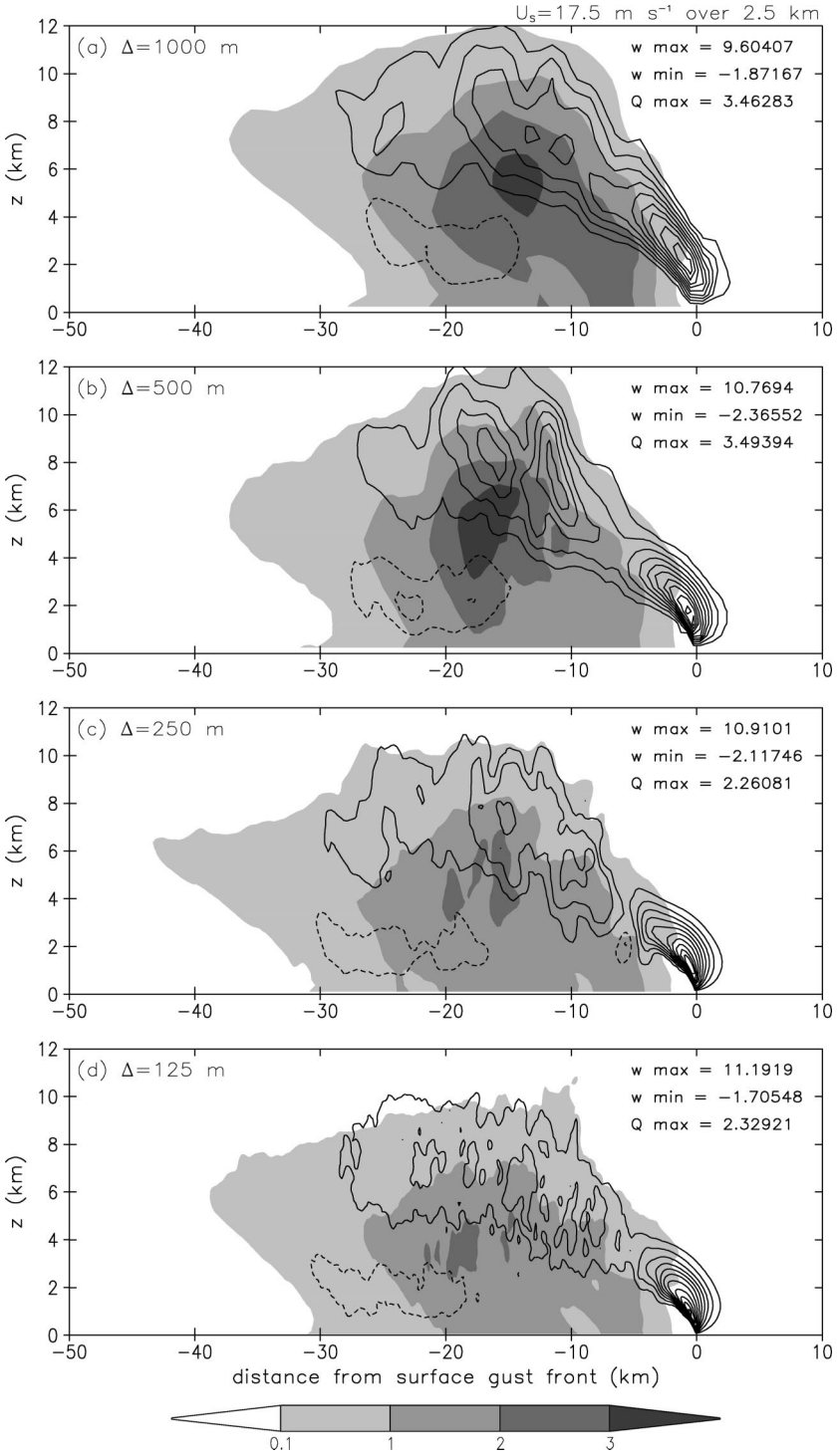

FIG. 5. Line-averaged vertical cross sections at 180 min of vertical velocity (contoured) and rainwater mixing ratio (shaded) from strong-shear simulations using grid spacings of (a) 1000, (b) 500, (c) 250, and (d) 125 m. The location of the surface gust front is normalized to a common location before averaging. For vertical velocity, the contour interval is 1 m s^{-1}, with negative contours dashed, and the zero contour excluded.

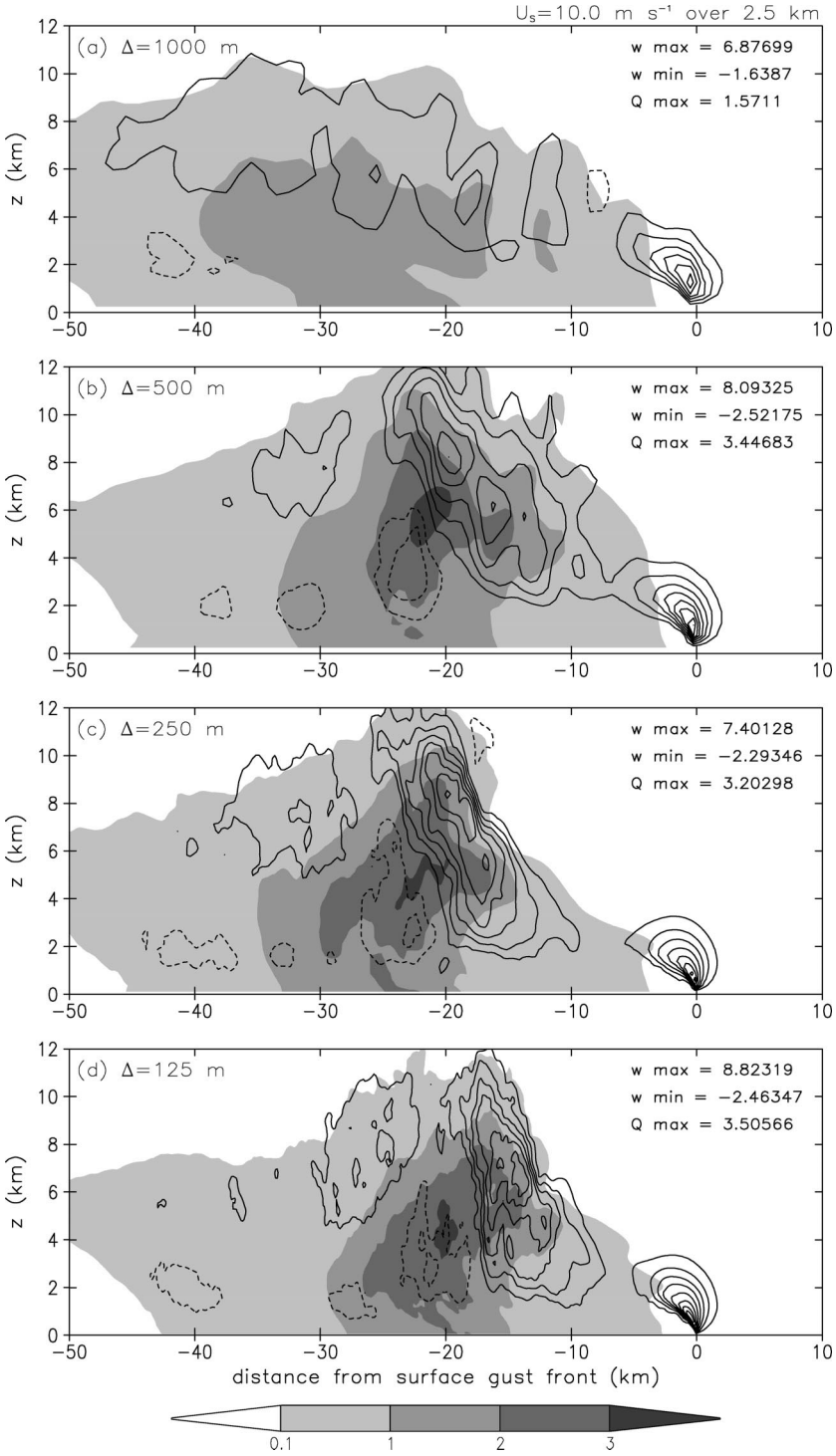

FIG. 6. The same as in Fig. 5 except for weak-shear simulations.

is required for the subgrid model to be appropriate—energy spectra from the strong-shear simulations are presented. One-dimensional vertical velocity spectra were computed in the *y* direction (i.e., along the convective line) at 5 km above ground. Since the squall-line structure varies considerably in the *x* direction, it is not meaningful to average spectra in this direction, as is typically done in studies of the atmospheric boundary layer (which is statistically homogenous in *both* horizontal directions). To obtain robust energy spectra,

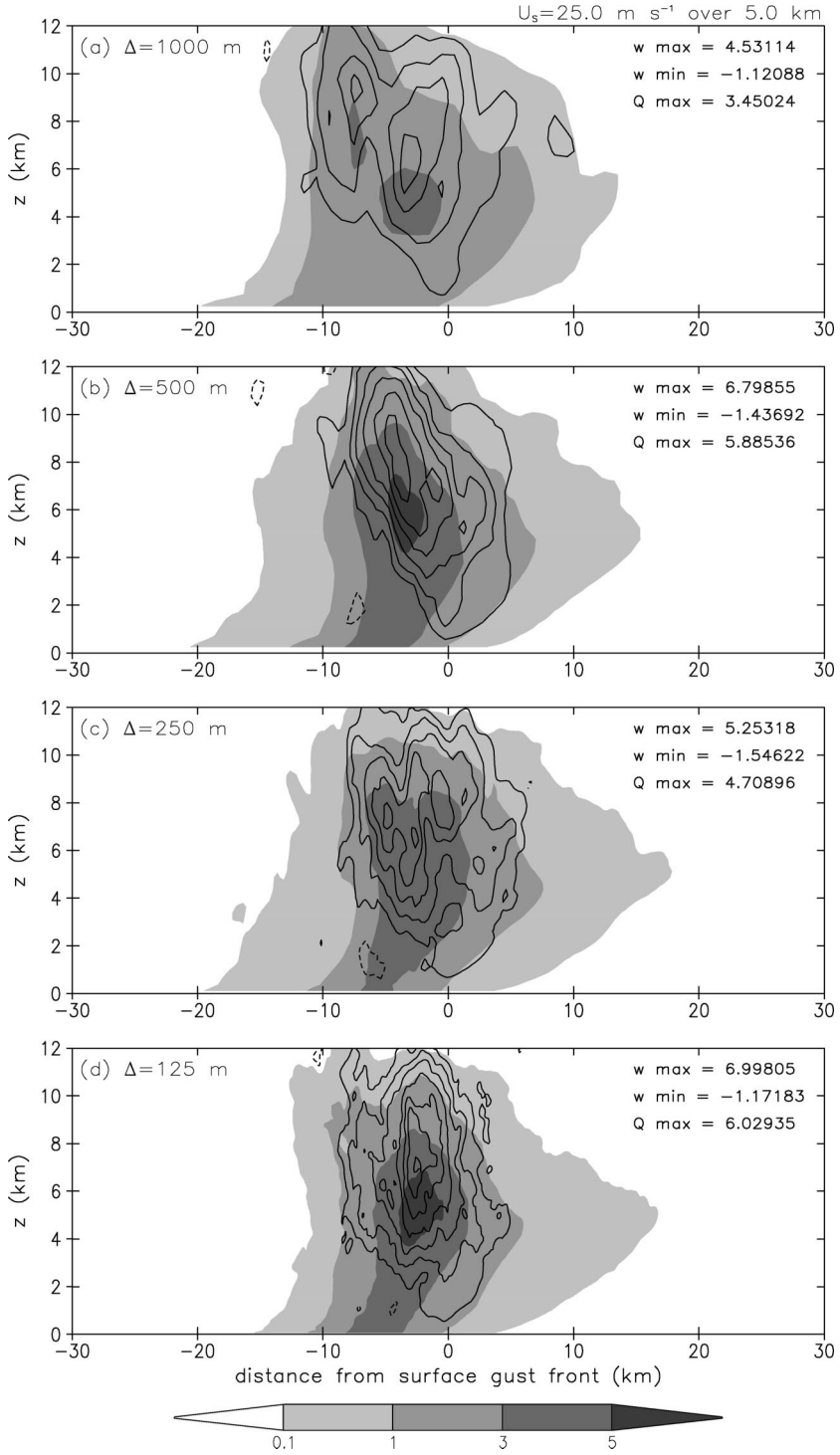

FIG. 7. The same as in Fig. 5 except for deep-shear simulations. Note that the shading increments are different from those used in Figs. 5 and 6.

while still averaging in a physically meaningful manner, the spectra presented here were determined by computing one spectrum per minute for 30 min and then temporally averaging. To ensure that roughly the same area of the squall line was being analyzed at each time, the spectra were computed at the *y* slice that had the highest vertical velocity variance at each time level, which at midlevels is always within the convective region of the squall line.

If assumption 1 is valid—that is, if an inertial sub-

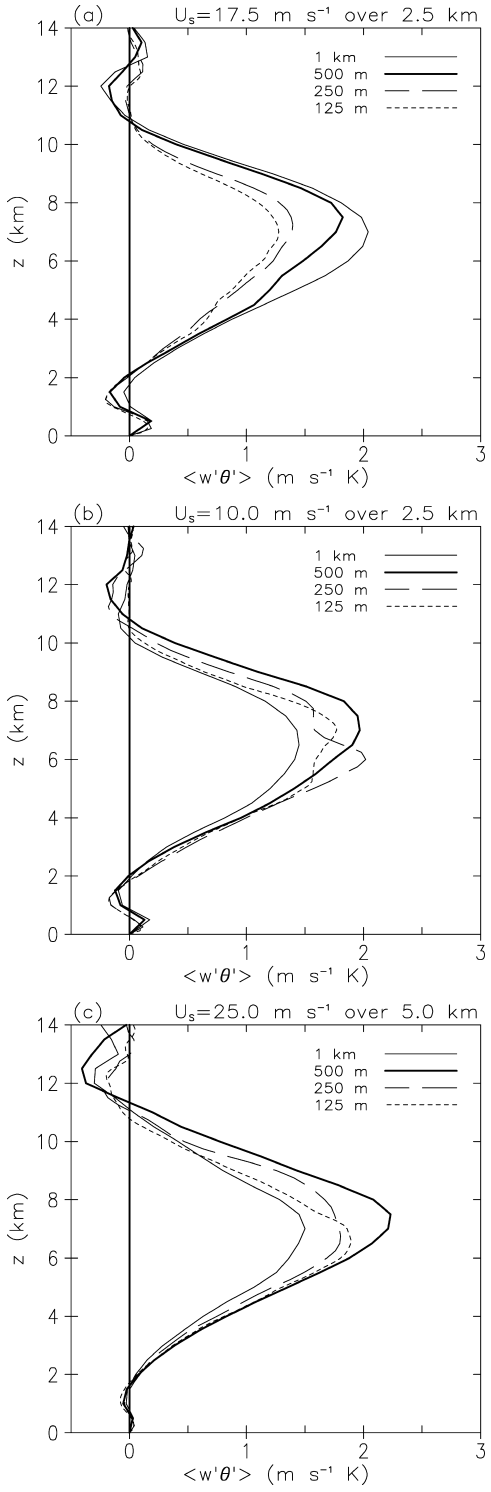

FIG. 8. Vertical profiles of $\langle w'\theta' \rangle$ (m s^{-1} K) for the various resolutions using (a) the strong-shear wind profile, (b) the weak-shear wind profile, and (c) the deep-shear wind profile. The four grid spacings are 1 km (thin solid line), 500 m (thick solid), 250 m (long-dashed), and 125 m (short-dashed). The averaging area extends from 50 km ahead of the surface gust front to 100 km behind the surface gust front.

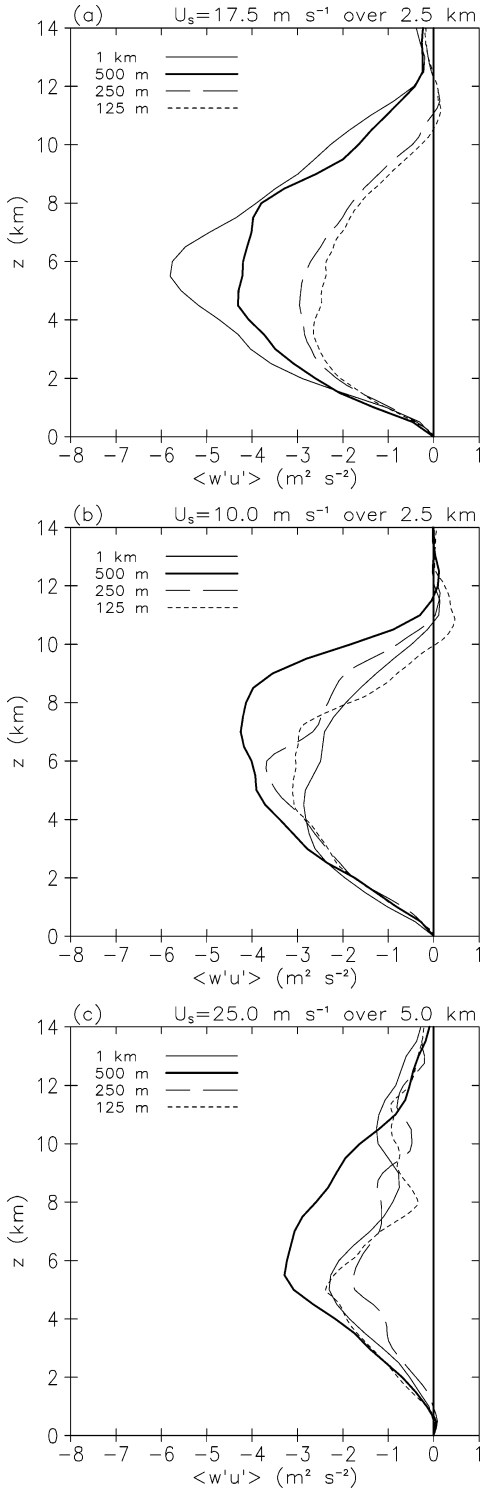

FIG. 9. The same as in Fig. 8 but vertical profiles of $\langle w'u' \rangle$ are plotted.

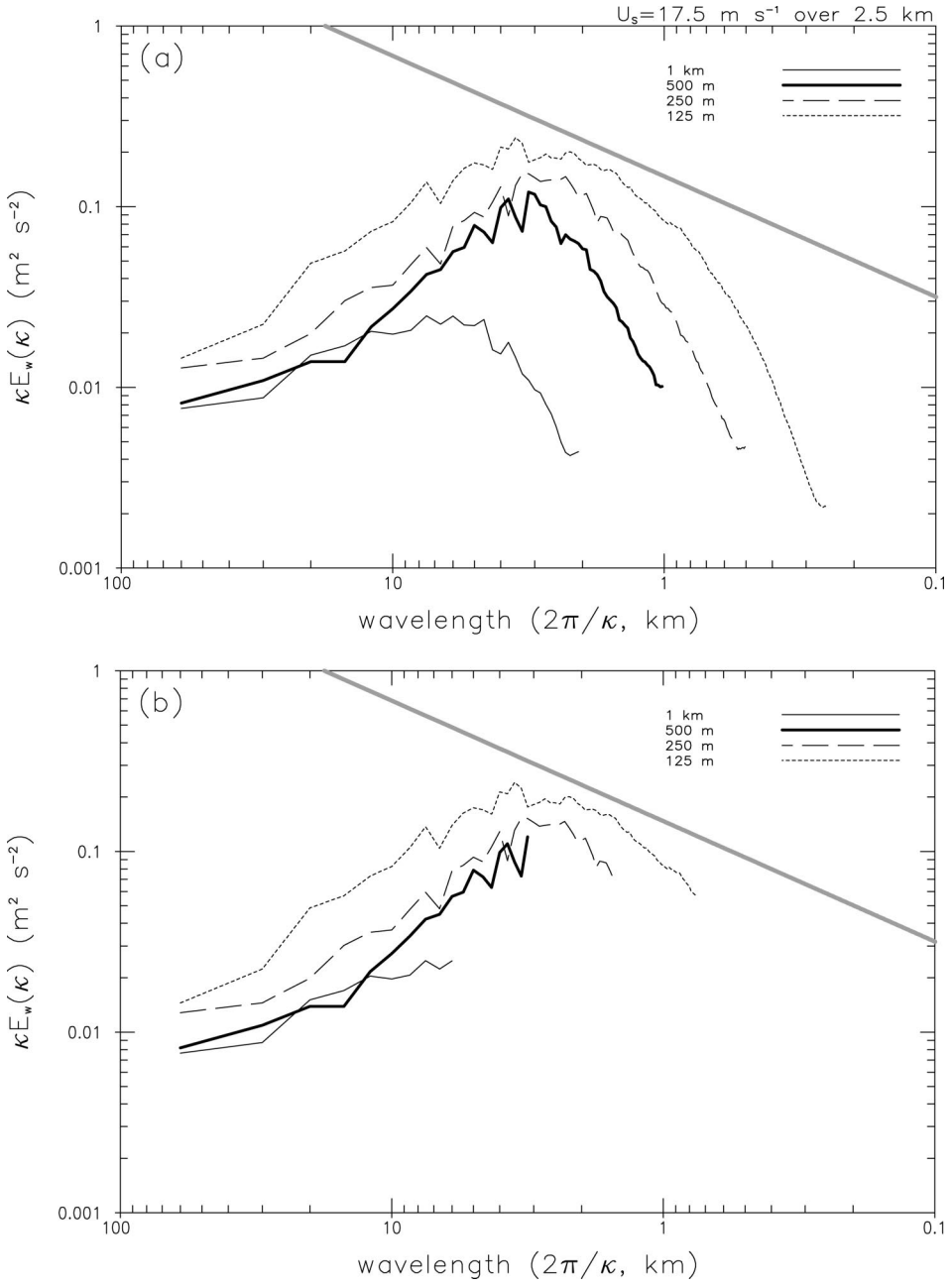

FIG. 10. One-dimensional (*y*-direction) vertical velocity spectra at 5 km above ground. The spectra were computed using output every minute for 30 min (150–180 min). A thick gray line corresponding to a $\kappa^{-5/3}$ spectrum is included to illustrate behavior that is expected in an inertial subrange. (b) Curves are the same as those in (a) except information at wavelengths less than 6Δ have been excluded.

range is present in the model runs—one would expect to have one-dimensional energy spectra that decrease with increasing wavenumber as $\kappa^{-5/3}$ beyond the energy-containing range. All four resolutions display this qualitative behavior (Fig. 10a), although the spectra are slightly shallower than $\kappa^{-5/3}$. On the other hand, the amplitude and wavelength of the energy peak systematically vary: the magnitude increases with increasing resolution, and the location of this maximum shifts to smaller scales.

As shown in Fig. 10a, it is possible to determine spectra for scales as small as 2Δ. Many figures in the literature do present this information. However, based on studies with different model configurations, we have concluded that information at scales smaller than 6Δ does not represent a physical solution for the model

design used here.[6] Although there is no explicit numerical filtering in these simulations, the fifth-order advection scheme utilized here inherently includes a sixth-order filter (Wicker and Skamarock 2002). Such a filter selectively damps features of wavelength less than 6Δ (Durran 1999). Through numerical experimentation, it was found that the slopes of the spectra below 6Δ are strongly affected by the intensity of the numerical filtering, and that information below 6Δ represents a *numerical* solution that is not relevant to the issues raised in section 3 (see the appendix for more information). Therefore, the vertical velocity spectra from Fig. 10a were also plotted with information at wavelengths less than 6Δ excluded; that is, only the physical portion of the spectra are displayed (Fig. 10b). When viewed in this manner, the nature of the various resolution simulations becomes clear. The two highest-resolution simulations (i.e., the runs with 250- and 125-m grid spacing) display the qualitative behavior that is expected in an inertial subrange, while the two lower-resolution runs do not (Fig. 10b). Hence, it can be concluded that the 125- and 250-m runs have an inertial subrange—and satisfy assumption 1—while the 500- and 1000-m runs do not. Not only do the coarser-resolution runs not have an inertial subrange, but the 1-km simulation does not even resolve accurately the spectral peak in kinetic energy, which provides further evidence that traditional LES techniques are not appropriate for grid spacings of order 1 km. In principle, one could design a subgrid closure for this regime. An appropriate closure for 1-km grid spacing should account for unresolved eddies with energy *greater* than that represented on the grid. (In contrast, the LES subgrid model that is used in the simulations is primarily designed to *extract* energy from the resolved scales).

The spectrum from the 125-m run has an inertial subrange spectrum slightly shallower than $\kappa^{-5/3}$. It is possible that the grid spacing is still not small enough to produce an adequately high Reynolds number. This argument is supported by the fact that assumption 2 is not satisfied; the large-eddy scale (l) determined from Fig. 10 is about 3 km, which is considerably smaller than the 10-km value used in the thought experiment at the end of section 3. To obtain a l/Δ ratio of about 100, a simulation with $\sim$30 m grid spacing would be required. With an appropriately high Reynolds number at this higher resolution [which follows from (12)], perhaps the spectrum would rise to $\kappa^{-5/3}$. A lack of a sufficiently high Reynolds number may also explain the lack of convergence noted in previous analyses. That is, according to Reynolds number similarity, convergence cannot occur until a threshold Reynolds number has been exceeded by all simulations (i.e., resolutions).

[6] This conclusion does not hold for all model formulations. For example, a pseudospectral model would be expected to contain a physical solution at much smaller scales.

e. Appropriateness of traditional LES closure

The appropriateness of using traditional LES closure with 1-km grid spacing is further addressed by analyzing the subgrid kinetic energy and subgrid fluxes produced in the various simulations. As mentioned earlier, traditional LES assumes that a large percentage of the kinetic energy and fluxes in a turbulent flow are resolved on the grid. Analyses were performed to address how well the various resolution simulations meet these criteria.

The subgrid turbulence kinetic energy, e^s, is predicted during the model run using the equations presented in Deardorff (1980). As in LES studies of the PBL, the resolved turbulence kinetic energy is defined as $e^r = [(u'')^2 + (v'')^2 + (w'')^2]/2$, where the double prime indicates the deviation from a horizontal average,

$$\alpha'' = \alpha^r - \langle \alpha^r \rangle, \tag{13}$$

α^r is the resolved variable of interest (such as u^r, v^r, w^r, etc.), and the angular brackets indicate a horizontal average. In this section, the spatial average is one-dimensional, and is defined to be the along-line average values relative to the position of the surface gust front. As an example, $\langle w^r \rangle$ and $\langle q_r^r \rangle$ are plotted in Figs. 5–7. The average field in this study is two-dimensional (x,z), which is in contrast to studies of the PBL where average fields are typically one-dimensional (z). The methodology here removes the mesoscale squall-line circulation, since this overturning is not relevant to the issues being addressed here.

To examine the appropriateness of the LES methodology, the ratio of the along-line average subgrid turbulence kinetic energy to total turbulence kinetic energy,

$$\frac{\langle e^s \rangle}{\langle e^r \rangle + \langle e^s \rangle}, \tag{14}$$

is plotted for all resolutions and initial shear profiles in Fig. 11. In LES, it is desirable to have a low ratio ($\sim$10% or lower). For the simulations with grid spacing of 1000 m, this condition is not met (Figs. 11a,e,i); the ratio exceeds 20% up to 6 km above ground in the convective region, and exceeds 70% above the gust front. Output from the deep-shear simulation produces the best results, although broads regions of ratio greater than 20% still exist in the mean (Fig. 11i).

As resolution is increased, the ratio of subgrid energy to total energy systematically decreases in magnitude and area for all shears (Fig. 11). With 125 m, this ratio slightly exceeds 10% over portions of the convective region, which is generally considered acceptable for LES. Again, the deep-shear simulation exhibits the lowest mean ratios (Fig. 11l). Rather large ratios are sometimes found just above the surface gust front, especially in the weak-shear simulation (Fig. 11h). This is the region where broad swaths of moist absolute instability are created (Bryan and Fritsch 2000; Bryan 2002). These layers tend to be 1–3 km deep, and can be very

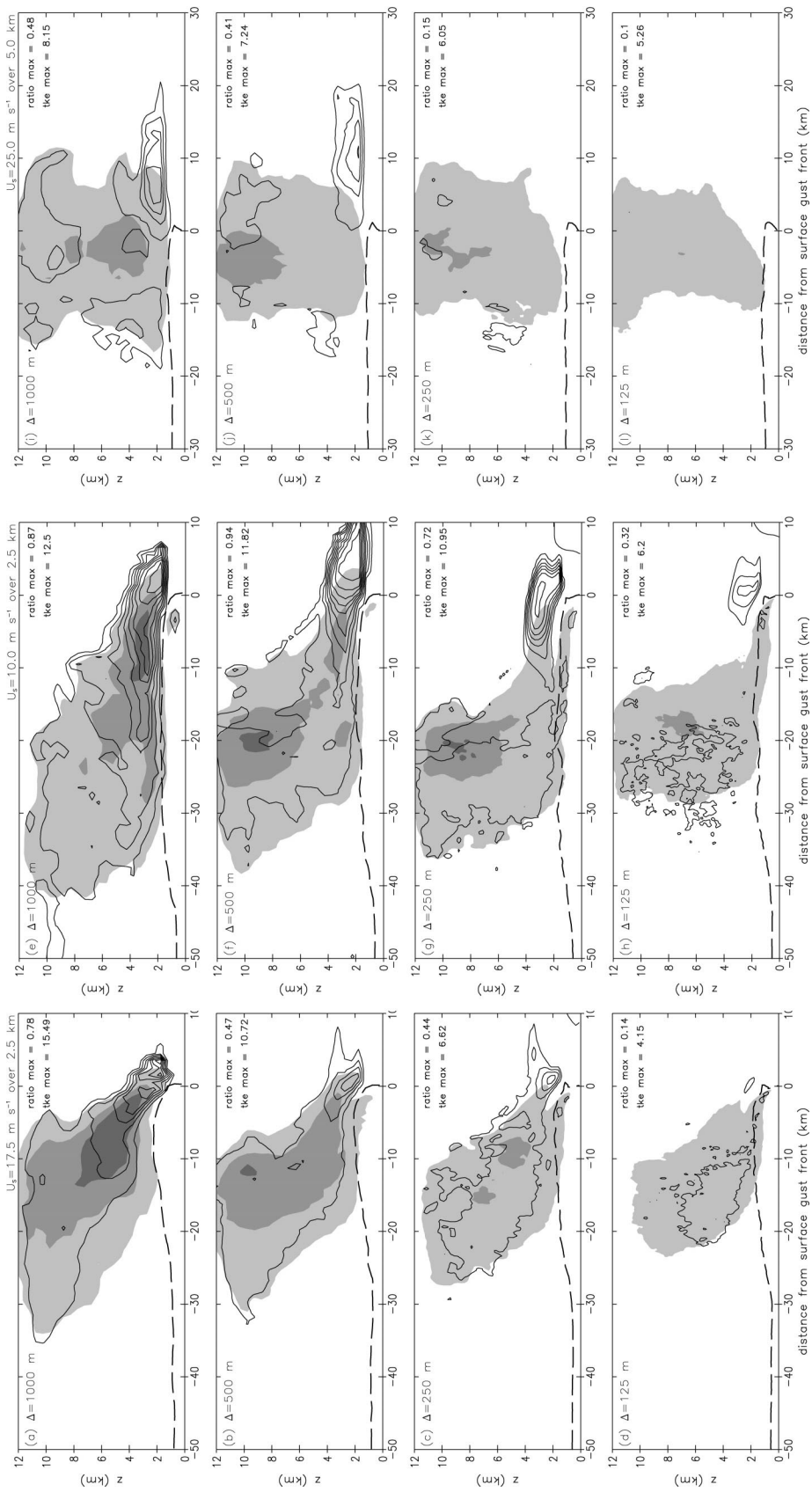

FIG. 11. Line-averaged cross sections of subgrid turbulence kinetic energy (TKE, shaded) and the ratio of subgrid TKE to total TKE (contours). For subgrid TKE, the three levels of shading correspond to, from lightest to darkest, 1–5, 5–10, and >10 m^2 s^{-2}. For the ratio of subgrid TKE to total TKE, the contour interval is 0.1, with the zero contour excluded. The −1 K potential temperature perturbation is included as a dashed black contour, which indicates the approximate position of the surface-based cold pool. (a)–(d) Results using strong shear, (e)–(h) using weak shear, and (i)–(l) results using deep shear. A Grid spacing of 1000 m was used for (a), (e), and (i); 500 m was used for (b), (f), and (j); 250 m was used for (c), (g), and (k); and 125 m was used for (d), (h), and (l).

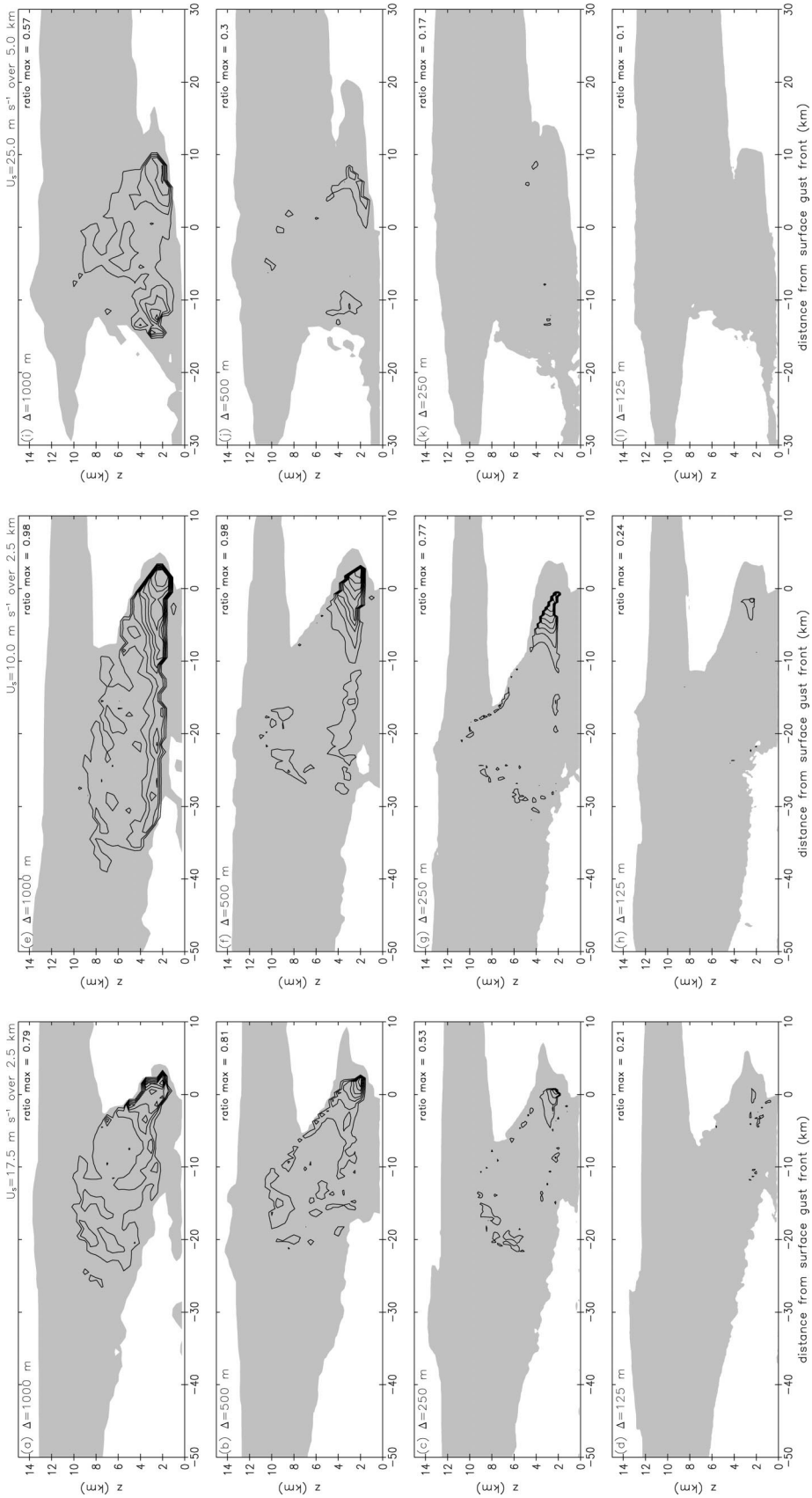

FIG. 12. Line-averaged cross sections of cloudwater greater than 1×10^{-5} kg kg^{-1} (shaded) and the ratio of subgrid turbulent water flux to total turbulent water flux (contours, with a contour interval of 0.1, and the zero contour excluded). (a)–(d) Results using strong shear, (e)–(h) using weak shear, and (i)–(l) using deep shear. A grid spacing of 1000 m was used for (a), (e), and (i); 500 m was used for (b), (f), and (j); 250 m was used for (c), (g), and (k); 125 m was used for (d), (h), and (l).

unstable, with lapse rates greater than 10 K km^{-1} in saturated conditions. Since the length scale of these unstable layers is about the same as the depth of the planetary boundary layer, it may be necessary to use O(10 m) grid spacing to resolve turbulence here.

The along-line averages of e^s (shaded in Fig. 11) decrease in magnitude and (generally) decrease in areal extent as resolution is increased. One interesting aspect of the highest-resolution simulations is the existence of high values of e^s within the cold pool just behind the surface gust front (see, e.g., the shading in the cold pool in Figs. 11d and 11h). A corresponding feature is virtually absent from the 1-km simulations, particularly from the strong-shear run (Fig. 11a). Further analysis reveals that these high e^s regions develop in locally intense shearing zones associated with Kelvin–Helmholtz billows near the top of the cold pool. Bryan (2002) showed that Kelvin–Helmholtz rolls can modify the properties of the cold pool, which, in turn, modifies the evolution of the convective system. These rolls do not occur with grid spacing of 1 km, revealing another reason why 1-km grid spacing is insufficient to accurately reproduce convective processes in squall lines.

A comparison of the 250- and 125-m simulations reveals another possible reason why convergence has not been achieved between these two resolutions. That is, in the 250-m simulation the ratio of subgrid energy to total energy is still rather high, and covers larger areas. It can be concluded that a well-founded LES regime has still not been reached with 250-m grid spacing—at least not over the entire squall line. This conclusion is corroborated by the energy spectra presented earlier; although the 250-m simulation resolves an inertial subrange, its extent is rather short—only about ¼ of a decade (Fig. 10b).

An analysis of total water flux is also provided to address the resolution of turbulent fluxes of scalars in deep moist convection. The vertical component of subgrid total water flux is parameterized in the model as

$$\tau_{q_t} = -K_h \frac{\partial q_t}{\partial z}, \tag{15}$$

where K_h is the subgrid coefficient for scalars, and $q_t = q_v + q_c + q_r$ is the total water mixing ratio (the sum of mixing ratios of vapor, cloudwater, and rainwater). The resolved turbulent water flux is $w''q_t''$. The ratio of along-line average subgrid flux to average total flux,

$$\frac{\langle \tau_{q_t} \rangle}{\langle \tau_{q_t} \rangle + \langle w''q_t'' \rangle}, \tag{16}$$

is plotted for all resolutions and shear profiles in Fig. 12. As with the ratios of kinetic energy, the ratios of water flux are inappropriately large in the 1-km simulations over broad regions. As resolution is increased, the ratio decreases to acceptable values. In fact, the ratios are almost everywhere less than 10% in the 125-m simulations: the exception, again, being within the layers of moist absolute instability that form over the gust front. Nevertheless, from a moisture flux perspective, grid spacing of order 100 m is clearly sufficient to satisfy the basic assumptions of LES.

6. Summary

Appropriate resolution for simulating deep moist convection is addressed from a turbulence perspective. Scale analysis reveals that grid spacing of order 0.1 mm may be required to simulate all scales of a geophysical turbulent flow. Since this resolution far exceeds the capabilities of existing computers, another approach is necessary. If the turbulent field is spatially filtered, thereby removing small-scale dissipative eddies, the computing requirements become manageable. However, the governing equation for a filtered flow contains unknown subgrid terms that must be parameterized. The large-eddy simulation (LES) technique is analyzed in this paper because it has been used to successfully simulate a wide variety of turbulent flows, and because it has been used in cloud-resolving models (CRMs) for decades.

Examination of the assumptions inherent in LES, and an analysis of the appropriate length scales, suggests that grid spacing on the order of 100 m is required for turbulence schemes used in CRMs to be appropriate. Based on these arguments, numerical simulations of squall lines were conducted with grid spacings of 1 km, and 500, 250, and 125 m. In these simulations, specific details of the squall line change significantly as the resolution is increased. In particular, precipitation distribution and amount, phase speed, cloud depth, mesoscale flow patterns, and stability structure all change substantially. Further analysis led to the following conclusions:

- With grid spacing of order 1 km, overturning occurs in a relatively *laminar* manner. Using grid spacing of order 100 m, the simulated fields are *turbulent*, with resolved entrainment and overturning within clouds.
- The highest-resolution simulations reveal that deep moist convection may be 1–2 km in scale in some conditions. Therefore, the ''rule of thumb'' that 1 km is sufficient to resolve deep moist convection can be inappropriate in some environments.
- In some instances, changing grid spacing from 1 km to 125 m changes the mode of convective overturning. In one example, the convection changes from a series of upright convective cells to a single sloped, plume-like cell with undilute ascent along the axis of the plume.
- Using filtering and along-line averaging, it is concluded that simulations with 1-km grid spacing are not producing equivalent squall-line structure and evolution as compared to the higher-resolution simulations.
- The trend in specific fields seems to be unpredictable,

with mean vertical velocity and rainwater values increasing with higher resolution in some environments, but decreasing with higher resolution in others.
- Systemwide flux profiles reveal that simulations with 1-km grid spacing do not always compare well with higher-resolution simulations, indicating that 1-km grid spacing cannot be used as a ''benchmark'' or ''control'' solution in resolution sensitivity studies.
- Energy spectra at midlevels reveal that only the 250- and 125-m simulations contain an inertial subrange. These results confirm that traditional LES closures are not appropriate with grid spacing of order 1 km.
- The ratio of subgrid turbulence energy to total turbulence energy further confirms that traditional LES techniques are inappropriate for grid spacing of order 1 km. On average, this ratio exceeds 10% throughout most of the squall line. As resolution is increased, the maximum values and areal extent of this ratio gradually decreases to acceptable values. A similar conclusion holds for an analysis of total water flux.

In summary, it is concluded that traditional LES closures cannot be used to simulate faithfully deep moist convection with grid spacing of order 1 km. This does not imply a problem with the subgrid model; rather, it is the common application of this model that is problematic. To be precise, it is argued that cloud-resolving models, *as currently formulated*, are not suitable for grid spacing of order 1 km. The results here suggest that grid spacing of order 100 m *is* appropriate, although further study with grid spacing of 50 m or less is necessary to clarify some issues.

7. Discussion

Some of the analyses here portray a strongly negative view of simulations with 1-km grid spacing. In particular, the analysis of energy spectra and the magnitude of subgrid energy and subgrid water fluxes clearly display behavior that is unacceptable for the model design. Nevertheless, it is noted that the 1-km simulations are able to reproduce the basic squall-line circulation itself, even if some details are incorrect. In fact, the quantitative and qualitative differences between the 1-km and 125-m simulations are much less than the differences Weisman et al. (1997) noted between simulations with 1- and 12-km horizontal grid spacing. This is an important point for the operational forecasting community, because simulations with quasi-cloud-resolving grid spacings of 1–4 km are now feasible in real time. Although it may not be possible to accurately predict some details of convection with 1-km grid spacing—such as precipitation distribution and amount, and system propagation speed—it could be argued that explicit modeling of convective systems can (and does) provide useful information to forecasters.

On the other hand, the research community frequently uses model output in lieu of observations—as is often the case for studies of deep moist convection. We argue that a model configuration that is well founded should be desired for this purpose. Simulations with O(100 m) grid spacing provide a greater confidence in the fidelity of the quantitative results. Furthermore, it is recommended that simulations with 100-m grid spacing should be used as benchmark or control simulations in resolution sensitivity studies. These simulations also raise serious doubts concerning the use of simulations with O(1 km) grid spacing to develop cumulus parameterizations schemes, as advocated by Browning et al. (1993) and Bechtold et al. (2000). For example, in Figs. 8 and 9, the maximum values of the flux profiles change by 25%–100% as resolution is increased. If output from O(1 km) simulations cannot be evaluated first against observations (as suggested by Redelsperger et al. 2000), then we would recommend against using the data to develop cumulus parameterizations.

We have found that using O(100 m) grid spacing provides a richer, more detailed, and more realistic perspective on the processes that occur in deep moist convection. For example, the existence of resolved entrainment and overturning clearly provides a more realistic picture on how convection interacts with its environment. In addition, with 100-m grid spacing it becomes possible to resolve certain organized modes of overturning, such as Kelvin–Helmholtz waves. Based on our experience, we argue that conclusions drawn from O(100 m) simulations can differ markedly from conclusions drawn using coarser, nonturbulent O(1 km) simulations.

An essential point here is that by going to resolutions of O(100 m), one enables the physical process of cloud turbulence to occur in simulations of moist convection. This process is an inherent element of convective overturning and is therefore essential in any realistic representation of convective processes. It follows that meaningful simulations of convective processes should be performed with resolutions of O(100 m).

8. Future work

The lack of convergence with increasing resolution noted here may be related to deficiencies in the subgrid model. Cotton (1975) pointed out several inadequacies in using the traditional Smagorinsky–Lilly–Deardorff model for simulating deep, moist convection. He suggested replacing the traditional LES scheme with higher-order turbulence schemes. In support of this conclusion, Redelsperger and Sommeria (1986) found that ''a well-designed parameterization scheme can compensate for some of the model inaccuracies which inevitably arise from a coarse [O(1 km) grid spacing] resolution.'' Therefore, in lieu of endlessly pursuing higher resolution, perhaps future studies should explore the resolution dependence of simulated convection using nontraditional subgrid models. As a first step, one could investigate the role of backscatter—the transfer of energy

from subgrid scales to resolved scales—on simulations of deep moist convection. Mason and Thompson (1992) found that a model including backscatter improved simulations of the stable atmospheric boundary layer, but had negligible impact on simulations of buoyant boundary layers. This suggests that backscatter effects may not be important in the convective region of squall lines, which has been the focus of this study.

Future studies should also explore the resolution sensitivity of different types of convection, such as an unorganized complex of convective cells or perhaps a line of supercells. It is unknown whether the choice of simulating squall lines for this study affects the generality of the conclusions. Furthermore, the simulations herein evolve independently of any background forcing, such as that provided by synoptic forcing, terrain, and/or land surface features. Background forcing may help mitigate some of the differences with resolution that have been noted here (such as differences in propagation speed of a convective system).

The role that the microphysics scheme plays in the sensitivity of simulations of moist convection is another uncertainty in the present simulations. Recent studies by Adlerman and Droegemeier (2002) and Gilmore et al. (2003, manuscript submitted to *Mon. Wea. Rev.*) document a strong sensitivity in convective evolution to microphysical formulations, suggesting that the predictability of moist convection is more than just a problem of inadequate resolution. Furthermore, recent studies have documented that certain microphysical equations have a resolution bias (e.g., Stevens et al. 1996; Larson et al. 2001), which may be playing a role in the lack of convergence noted here. This suggests the need to conduct simulations with a resolution-independent microphysical scheme (which may not currently exist).

Acknowledgments. Computing resources for this study were provided by the National Center for Atmospheric Research, which is sponsored by the National Science Foundation. This work was supported by NSF Grants ATM 9806309 and ATM 0133506. All figures were created using the Grid Analysis and Display System (GrADS).

APPENDIX

Sensitivity of Energy Spectra to Numerical Diffusion

As discussed in section 5d, we have concluded that only information at scales greater than 6Δ in energy spectra represent a physical solution for our model configuration. In support of this conclusion, a series of simulations was conducted using 125-m grid spacing and the same model setup, but over a smaller (24 km $\times$ 24 km) domain. These simulations were initialized with a cold pool rather than a warm thermal to accelerate the initial overturning (see Bryan and Fritsch 2001 for the exact model initialization). Rather than using a fifth-order approximation for advection, which has an inherent dissipation that is proportional to wind speed and inversely proportional to grid spacing, a sixth-order approximation to advection was used here. To control numerical noise, an explicit sixth-order filter was applied

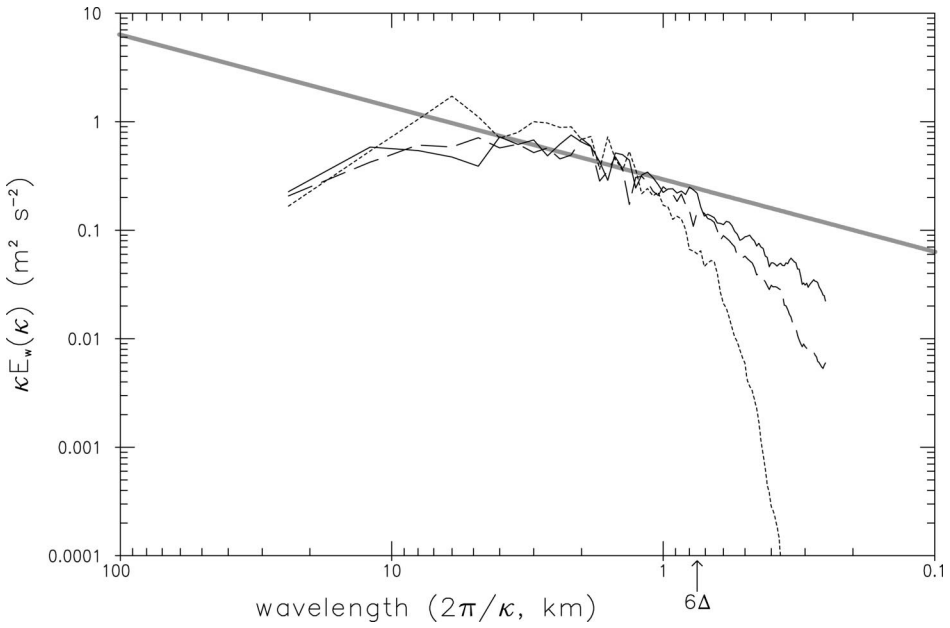

FIG. A1. As in Fig. 10a, except only simulations with 125-m grid spacing are analyzed, and the spectra were computed from 30 to 60 min. The three simulations used sixth-order nondimensional diffusion coefficients of 3.125×10^{-4} (solid), 1.5625×10^{-3} (long-dashed), and 1.484×10^{-2} (short-dashed).

every time step. By varying the constant coefficient in the explicit filter, physical and computational portions of the spectra became apparent (Fig. A1). The physical spectrum extends from the largest scales (24 km here) to a wavelength corresponding to $\sim 6\Delta$; this portion of the spectrum remains essentially unchanged as the numerical filtering coefficient is varied. In contrast, the computational portion, which extends from wavelengths of $\sim 6\Delta$ to wavelengths of 2Δ, varies considerably as the magnitude of smoothing is modified. Thus, it is possible to create whatever spectral slope the user wishes below 6Δ (with this configuration) by changing the magnitude of numerical diffusion in the model. The fifth-order advection scheme used for the main simulations of this study is a combination of a sixth-order advection scheme and a sixth-order filter (Wicker and Skamarock 2002); it follows that information above 6Δ in the spectra represents a physical solution, while information below 6Δ represents a numerical solution that is not relevant to the issues raised in section 3.

A study by Harris et al. (2001) further supports this conclusion. They compared output from an explicit ($\Delta = 3$ km) simulation of a line of convection to radar data of the same case. A power spectrum analysis of the precipitation fields revealed excellent comparison from large scales to a scale of about 5Δ. Harris et al. (2001) conclude that only information at scales greater than approximately 5Δ should be considered useful for most applications. They also conclude, in agreement with the present study, that numerical diffusion (both implicit and explicit) in numerical modeling systems is responsible for the falloff in variability at small scales.

REFERENCES

Adlerman, E. J., and K. K. Droegemeier, 2002: The sensitivity of numerically simulated cyclic mesocyclogenesis to variations in model physical and computational parameters. *Mon. Wea. Rev.*, **130,** 2671–2691.

Bechtold, P., and Coauthors, 2000: A GCSS intercomparison for a tropical squall line observed during TOGA-COARE. II: Intercomparison of single-column models and a cloud-resolving model. *Quart. J. Roy. Meteor. Soc.*, **126,** 865–888.

Bluestein, H. B., 1986: Fronts and jet streaks: A theoretical perspective. *Mesoscale Meteorology and Forecasting*, P. S. Ray, Ed., Amer. Meteor. Soc., 173–215.

Browning, K. A., and the GEWEX Cloud System Science Team,1993: The GEWEX Cloud System Study (GCSS). *Bull. Amer. Meteor. Soc.*, **74,** 387–399.

Bryan, G. H., 2002: An investigation of the convective region of numerically simulated squall lines. Ph.D. thesis, The Pennsylvania State University, 181 pp.

——, and J. M. Fritsch, 2000: Moist absolute instability: The sixth static stability state. *Bull. Amer. Meteor. Soc.*, **81,** 1207–1230.

——, and ——, 2001: On adequate resolution for the simulation of deep moist convection: Theory and preliminary simulations. Preprints, *Ninth Conf. on Mesoscale Processes*, Fort Lauderdale, FL, Amer. Meteor. Soc., 288–292.

——, and ——, 2002: A benchmark simulation for moist nonhydrostatic numerical models. *Mon. Wea. Rev.*, **130,** 2917–2928.

Corrsin, S., 1961: Turbulent flow. *Amer. Sci.*, **49,** 300–325.

Cotton, W. R., 1975: Theoretical cumulus dynamics. *Rev. Geophys. Space Phys.*, **13,** 419–448.

Deardorff, J. W., 1970a: A three-dimensional numerical study of turbulent channel flow at large Reynolds numbers. *J. Fluid Mech.*, **41,** 453–480.

——, 1970b: Preliminary results from numerical integrations of the unstable boundary layer. *J. Atmos. Sci.*, **27,** 1209–1211.

——, 1970c: Convective velocity and temperature scales for the unstable planetary boundary layer and for Rayleigh convection. *J. Atmos. Sci.*, **27,** 1211–1213.

——, 1980: Stratocumulus-capped mixed layer derived from a three-dimensional model. *Bound.-Layer Meteor.*, **18,** 495–527.

Droegemeier, K. K., G. Bassett, and M. Xue, 1994: Very high-resolution, uniform-grid simulations of deep convection on a massively parallel computer: Implications for small-scale predictability. Preprints, *10th Conf. on Numerical Weather Prediction*, Portland, OR, Amer. Meteor. Soc., 376–379.

——, ——, and D. K. Lilly, 1996: Does helicity really play a role in supercell longevity? Preprints, *18th Conf. on Severe Local Storms*, San Francisco, CA, Amer. Meteor. Soc., 205–209.

——, Y. P. Richardson, G. M. Bassett, and A. Marroquin, 1997: Three-dimensional numerical simulations of turbulence generated in the near-environment of deep convective storms. Preprints, *Seventh Conf. on Aviation, Range, and Aerospace Meteorology*, Long Beach, CA, Amer. Meteor. Soc., 169–174.

Durran, D. R., 1999: *Numerical Methods for Wave Equations in Geophysical Fluid Dynamics.* Springer-Verlag, 465 pp.

——, and J. B. Klemp, 1983: A compressible model for the simulation of moist mountain waves. *Mon. Wea. Rev.*, **111,** 2341–2361.

Gilmore, M. S., J. M. Straka, and E. N. Rasmussen, 2003: Precipitation and evolution sensitivity in simulated deep convective storms: Comparisons between liquid-only and simple ice and liquid phase microphysics. *Mon. Wea. Rev.*, submitted.

Grabowski, W. W., X. Wu, M. W. Moncrieff, and W. D. Hall, 1998: Cloud-resolving modeling of cloud systems during Phase III of GATE. Part II: Effects of resolution and the third spatial dimension. *J. Atmos. Sci.*, **55,** 3264–3282.

Harris, D., E. Foufoula-Georgiou, K. K. Droegemeier, and J. J. Levit, 2001: Multiscale statistical properties of a high-resolution precipitation forecast. *J. Hydrometeor.*, **2,** 406–418.

Kessler, E., 1969: *On the Distribution and Continuity of Water Substance in Atmospheric Circulation, Meteor. Monogr.*, No. 32, Amer. Meteor. Soc., 84 pp.

Klemp, J. B., and R. B. Wilhelmson, 1978: The simulation of three-dimensional convective storm dynamics. *J. Atmos. Sci.*, **35,** 1070–1096.

Kolmogorov, A. N., 1941: The local structure of turbulence in incompressible viscous fluid for very large Reynolds numbers. *Dokl. ANSSSR*, **30,** 301–305.

Larson, V. E., R. Wood, P. R. Field, J.-C. Golaz, T. H. Vonder Haar, and W. R. Cotton, 2001: Systematic biases in the microphysics and thermodynamics of numerical models that ignore subgrid-scale variability. *J. Atmos. Sci.*, **58,** 1117–1128.

Leonard, A., 1974: Energy cascade in large-eddy simulations of turbulent flows. *Advances in Geophysics*, Vol. 18A, Academic Press, 237–248.

Lilly, D. K., 1967: The representation of small-scale turbulence in numerical simulation experiments. *Proc. IBM Scientific Symp. on Environmental Sciences*, Yorktown Heights, NY, IBM DP Division, 195–210.

——, G. Bassett, K. Droegemeier, and P. Bartello, 1998: Stratified turbulence in the atmospheric mesoscales. *Theor. Comput. Fluid Dyn.*, **11,** 139–153.

Mason, P. J., and D. J. Thompson, 1992: Stochastic backscatter in large-eddy simulations of boundary layers. *J. Fluid Mech.*, **242,** 51–78.

——, and A. R. Brown, 1999: On subgrid models and filter operations in large eddy simulations. *J. Atmos. Sci.*, **56,** 2101–2114.

Moeng, C.-H., 1984: A large-eddy-simulation model for the study of planetary boundary-layer turbulence. *J. Atmos. Sci.*, **41,** 2052–2062.

Petch, J. C., and M. E. B. Gray, 2001: Sensitivity studies using a

cloud-resolving model simulation of the tropical west Pacific. *Quart. J. Roy. Meteor. Soc.,* **127,** 2287–2306.

——, A. R. Brown, and M. E. B. Gray, 2002: The impact of horizontal resolution on the simulations of convective development over land. *Quart. J. Roy. Meteor. Soc.,* **128,** 2031–2044.

Redelsperger, J. L., and G. Sommeria, 1986: Three-dimensional simulation of a convective storm: Sensitivity studies on subgrid parameterization and spatial resolution. *J. Atmos. Sci.,* **43,** 2619–2635.

——, and Coauthors, 2000: A GCSS model intercomparison for a tropical squall line observed during TOGA-COARE. I: Cloud-resolving models. *Quart. J. Roy. Meteor. Soc.,* **126,** 823–863.

Rogallo, R. S., and P. Moin, 1984: Numerical simulation of turbulent flows. *Ann. Rev. Fluid Mech.,* **16,** 99–137.

Smagorinsky, J., 1963: General circulation experiments with the primitive equations. *Mon. Wea. Rev.,* **91,** 99–164.

Stevens, B., R. L. Walko, W. R. Cotton, and G. Feingold, 1996: The spurious production of cloud-edge supersaturations by Eulerian models. *Mon. Wea. Rev.,* **124,** 1034–1041.

Stevens, D. E., A. S. Ackerman, and C. S. Bretherton, 2002: Effects of domain size and numerical resolution on the simulation of shallow cumulus convection. *J. Atmos. Sci.,* **59,** 3285–3301.

Straka, J. M., R. B. Wilhelmson, L. J. Wicker, J. R. Anderson, and K. K. Wilhelmson, 1993: Numerical solutions of a non-linear density current: A benchmark solution and comparisons. *Int. J. Numer. Methods Fluids,* **17,** 1–22.

Tannehill, J. C., D. A. Anderson, and R. H. Pletcher, 1997: *Computational Fluid Mechanics and Heat Transfer.* Taylor & Francis, 792 pp.

Tennekes, H., and J. L. Lumley, 1972: *A First Course in Turbulence.* M.I.T. Press, 300 pp.

Weisman, M. L., and J. B. Klemp, 1982: The dependence of numerically simulated convective storms on vertical wind shear and buoyancy. *Mon. Wea. Rev.,* **110,** 504–520.

——, W. C. Skamarock, and J. B. Klemp, 1997: The resolution dependence of explicitly modeled convective systems. *Mon. Wea. Rev.,* **125,** 527–548.

Wicker, L. J., and W. C. Skamarock, 2002: Time splitting methods for elastic models using forward time schemes. *Mon. Wea. Rev.,* **130,** 2088–2097.

Wilhelmson, R. B., and L. J. Wicker, 2001: Numerical modeling of severe local storms. *Severe Convective Storms, Meteor. Monogr.,* No. 50, Amer. Meteor. Soc., 123–166.

Wyngaard, J. C., 1982: Boundary layer modeling. *Atmospheric Turbulence and Air Pollution Modelling,* F. T. M. Nieuwstadt and H. van Dop, Eds., Reidel, 69–106.